



Nonbonding interaction analyses on PVDF/[BMIM][BF₄] complex system in gas and solution phase

Ranjini Sarkar¹ · T. K. Kundu¹

Received: 10 December 2018 / Accepted: 29 March 2019 / Published online: 25 April 2019
© Springer-Verlag GmbH Germany, part of Springer Nature 2019

Abstract

The present study provides a detailed quantum chemical description of the physicochemical interactions between poly-vinylidene fluoride (PVDF) and 1-butyl-3-methyl-imidazolium tetrafluoro borate ([BMIM][BF₄]) ionic liquid (IL). Geometry optimization and frequency calculations are carried out for four monomer units of α - and β -PVDF, [BMIM][BF₄], and PVDF/[BMIM][BF₄] using dispersion corrected density functional theory. The effects of solvation on the systems under study are demonstrated for three polar aprotic solvents, namely tetra-hydrofuran (THF), acetone, and n,n-dimethyl formamide (DMF) using the integral equation formalism polarizable continuum model (IEFPCM). Calculated negative solvation free energy values suggest solution phase stability of the systems under study. Binding and interaction energies for β -PVDF/IL are found higher in magnitude than those for α -PVDF/IL. The nonbonding interaction phenomenon of β -PVDF/[BMIM][BF₄] is elucidated on the basis of natural bond orbital (NBO), Bader's quantum theory of atoms in molecules (QTAIM), delocalization indices, Hirshfeld surface, and reduced density gradient (RDG) analyses. Both anions and cations of ionic liquids are found to show weak van der Waals interaction with PVDF molecule but the anion ([BF₄]⁻)/PVDF interaction is found to be stronger than cation ([BMIM]⁺)/PVDF interaction. Inter-unit C–H···F type hydrogen bonds are found to show improper (causing blue shifts in vibrational frequencies) nature. Frontier molecular orbital analysis is carried out, and different chemical parameters like electronegativity, chemical potential, chemical hardness and softness, and electrophilicity index are calculated using Koopmans' theorem. Thermochemical calculations are also performed, and the variation in different standard thermodynamic parameters with temperature is formulated.

Keywords PVDF/IL complex · Dispersion corrected DFT · Interaction energy · HOMO-LUMO · NBO · QTAIM · Delocalization index · Hirshfeld surface · NCI · RDG

Introduction

Electroactive polymers (EAP) have gained huge attention in the field of microelectronics because of their light weight, high flexibility, and ease of fabrication [1]. β -PVDF is one of the most discussed EAPs with high dipole moment and spontaneous polarization per monomer unit [2]. However, during PVDF synthesis, nonpolar α -PVDF is formed predominantly

[3] as it possesses lower energy (stable) trans-gauche configuration compared to the higher energy (unstable) all trans configuration of β -PVDF [3, 4]. Previously, mechanical stretching, electrical poling, and various high temperature-high pressure treatments were carried out to promote formation of β -PVDF crystals within α -PVDF blend [3–7]. However, several experimental studies [8–14] suggest that addition of different second phase materials (additives) is an effective method to induce β -PVDF crystallization from α -PVDF. Room temperature ionic liquids (RTILs) are one kind of these additives that help in β -PVDF formation as a result of strong ion–dipole interaction between IL and PVDF molecules [15, 16]. Highly miscible ILs work as plasticizers within the PVDF matrix [17] and form high performance dielectric composites, which are associated with excellent ductility, good optical transparency, enhanced ion electrical conductivity, and high dielectric constants [15–17]. Because of these enhanced properties, PVDF/IL composites are majorly

Electronic supplementary material The online version of this article (<https://doi.org/10.1007/s00894-019-4020-9>) contains supplementary material, which is available to authorized users.

✉ T. K. Kundu
tkkundu@metal.iitkgp.ac.in

¹ Department of Metallurgical and Materials Engineering, Indian Institute of Technology Kharagpur, Kharagpur, West Bengal 721302, India

applied in piezoelectric sensors, actuators, and energy storage devices [18]. Despite a satisfactory amount of experimental works, to the best of the author's knowledge, the theoretical explanation of the inter-unit interaction occurring within the PVDF/IL molecular complex still lacks enough attention. Besides, it is still debatable which part of the PVDF molecule interacts with which part of the ionic liquid (cation or anion). For example, according to Wang et al. [18], the interaction between polymer matrix and ionic liquid occurs through the anion of the IL and hydrogen atoms of PVDF. On the contrary, Liang et al. [19] claimed that the cation part of the ionic liquid plays the major role of interaction with the fluorine atoms within the PVDF molecule. The current study aims to clarify these facile remarks regarding the intra and inter-molecular interaction phenomenon occurring within PVDF/IL complex systems using dispersion corrected density functional theory (DFT-D) [20] based on linear combination of atomic orbitals (LCAO) approach [21]. DFT studies on PVDF/[C_nMIM][BF₄] (*n* = 2, 4, 6, 8, 10) were first performed and reported by the authors previously [22], where the effect of variation in the length (*n*) of the alkyl chain attached to the imidazolium ring of the ionic liquid cation was investigated. It was observed that the increase in length of the alkyl chain (in IL cation) actually does not help in altering different properties (e.g., charge distribution, frontier molecular orbital compositions, dipole moment, molecular electrostatic potential, etc.) at the molecular level. Therefore, to provide further insight into these complex systems only (α - and β -)PVDF/[C₄MIM][BF₄] molecules are taken and detailed analyses of nonbonding interactions are performed to describe the individual effect of anion and cation on the PVDF molecule. In spite of the higher stability of α -PVDF, ionic liquid added β -PVDF (β -PVDF/[BMIM][BF₄]) is found to be more stable than α -PVDF/[BMIM][BF₄] (explained later). Moreover, comparing the optimized structures of α -PVDF/[BMIM][BF₄] and β -PVDF/[BMIM][BF₄] with their respective initial structures, evidently, the positions of the constituting units of β -PVDF/IL are found to change drastically which indicates better interaction (dispersive) of β -PVDF with both anion and cation of the ionic liquid molecule [initial and final structures of α -PVDF/[BMIM][BF₄] and β -PVDF/[BMIM][BF₄] in the gas phase are given in the supplementary Fig. S1]. On the contrary, inter-unit interaction is found to be less in the case of the α -PVDF/IL system. Besides, according to the experimental findings mentioned earlier, addition of ionic liquid increases fractional content of β -PVDF compared to the α -phase. Therefore, it is more reasonable to emphasize on the inter fragment interactions occurring within the β -PVDF/IL system only. The exact region and intensity of nonbonding interactions are investigated for the cation [BMIM]⁺,

anion [BF₄]⁻ of the IL and β -PVDF part of the β -PVDF/IL complex using NBO analysis [23] (along with proper graphical representations of NBO interactions), Bader's QTAIM theory [24], calculation of delocalization indices [25], Hirshfeld surface analysis [26], NCI isosurface analysis, and RDG plot [27]. Besides, vibrational frequency analyses and thermochemical properties are introduced to provide better confirmation regarding the consistency of the current method with the experimental findings.

Synthesis of PVDF/IL composites requires a solvent medium. *N,N*-dimethyl formamide (DMF) is found as the most used solvent for PVDF based composites [28]. Therefore, to make the analyses more realistic, the effect of solvent addition on the systems under study has also been taken into account. Along with the gas phase calculations, solvent model calculations are carried out with three different polar aprotic solvents, namely tetrahydrofuran ($\epsilon = 7.4257$), acetone ($\epsilon = 20.493$) and *n,n*-dimethyl formamide ($\epsilon = 37.219$) using polarizable continuum model (PCM). PCM is an implicit solvent model, proposed by Tomasi et al. [29], where instead of considering individual solvent molecules (as in the case of explicit solvent models), all the solvent molecules are considered as a dielectric continuum of permittivity ϵ , within which the solute molecules are encapsulated in a cavity. An advanced PCM model, named integral equation formalism polarizable continuum model (IEFPCM) [30], is used here to describe the solvent continuum to provide a quantitative comparative estimate of the effect of the aforementioned solvents on the systems under study.

Computational details

All the density functional theory calculations are carried out using the Gaussian09 [31] program and Gaussview 5.0 [32] is used for visualization of the structures. Grimme's dispersion corrected DFT method (DFT-D) [20] is used to simulate four monomer units of α - and β -PVDF, ionic liquid [BMIM][BF₄], and the PVDF/[BMIM][BF₄] molecular complex. The DFT-D approach is considered to be very relevant to study the complex molecules as it takes into account the intra and inter unit interaction by incorporating a dispersion correction factor into the total energy term as obtained from standard density functional calculations and expressed as:

$$E_{\text{DFT-D}} = E_{\text{DFT}} + S \sum_{i \neq j} \frac{C_{ij}}{r_{ij}^6} f_{\text{damp}}(r_{ij}) \quad (1)$$

where r_{ij} is the distance between atoms 'i' and 'j', C_{ij} is the dispersion coefficient for atoms 'i' and 'j', $f_{\text{damp}}(r_{ij})$ is a damping function to avoid unphysical behavior of the dispersion term at small distances, and *S* is the scaling factor applied uniformly to all pairs of atoms. Dispersion correction has been

incorporated into the ‘standard functional’ (without dispersion) Becke’s nonlocal gradient-corrected three parameter exchange functional [33] with a correlation functional, as developed by Lee–Yang–Parr [34] (named B3LYP), and is used with polarized triple ξ basis set 6–311+G(d,p).

Binding energy (ΔE_b) values [35, 36] of PVDF/IL complexes are obtained using the following expression:

$$\Delta E_b = E_{PVDF+IL} - (E_{PVDF} + E_{IL}) \tag{2}$$

where $E_{PVDF+IL}$ = energy of optimized ionic liquid added β -PVDF molecule, E_{PVDF} = energy of optimized isolated β -PVDF molecule and E_{IL} = energy of optimized isolated ionic liquid molecule.

Basis set superposition error (BSSE) in the supermolecular interaction energy is calculated by counterpoise correction [37]. In this method, interaction energy (ΔE_i) is defined as:

$$\Delta E_i = E(AB, a \cup b, R) - [E(A, a, R) + E(B, b, R)] \tag{3}$$

BSSE corrected interaction energy is calculated as:

$$\Delta E_{i,corr} = E(AB, a \cup b, R) - [E(A, a \cup b, R) + E(B, a \cup b, R)] \tag{4}$$

where $E(AB, a \cup b, R)$, $E(A, a, R)$, and $E(B, b, R)$ are the energies of the AB complex, and A and B monomers, respectively. R is the geometry of the complex, and a, b, a \cup b are the basis set functions of A, B, and AB complex, respectively. In the present discussion, $A \equiv \alpha$ or β -PVDF, $B \equiv [BMIM][BF_4]$, and $AB \equiv PVDF/IL$ complex. BSSE correction is expressed as, $\Delta E - \Delta E_{i,corr}$

Another approach to obtain the interaction energy of a molecular complex is based on the symmetry adapted perturbation theory (SAPT) [38] where the interaction energy is calculated as the sum of perturbative corrections resulting from different physical effects (electrostatic, exchange, induction, and dispersion), without calculating the individual energy of the complex or its constituting units. In SAPT, the Hamiltonian of the complex (AB) is partitioned into contributions from each unit (A and B) and their interaction as follows:

$$H = F_A + W_A + F_B + W_B + V \tag{5}$$

where F_A and F_B are the Fock potentials of A and B, respectively, W_A and W_B are the fluctuation potentials of A and B, respectively, and V is the interaction potential.

Several SAPT methods are available that truncate the SAPT expansion of the interaction energy at the first and higher order of the perturbation operator. In the present work, only SAPT0 (the simplest truncation) and SAPT2 energies are calculated for the β -PVDF/[BMIM][BF₄] complex in the gas and solution phases using the PSI4 program [39]. Mathematical expressions of SAPT0 and SAPT2 energies are given as:

$$E_{SAPT0} = E_{elst}^{(10)} + E_{exch}^{(10)} + E_{ind,resp}^{(20)} + E_{exch-ind,resp}^{(20)} + E_{disp}^{(20)} + E_{exch-disp}^{(20)} + \delta_{HF}^{(2)} \tag{6}$$

$$E_{SAPT2} = E_{SAPT0} + E_{elst,resp}^{(12)} + E_{exch}^{(11)} + E_{exch}^{(12)} + E_{ind}^{(22)} + E_{exch-ind}^{(22)} \tag{7}$$

Notations ‘elst’, ‘exch’, ‘ind’, and ‘disp’ refer to the electrostatic, exchange, induction, and dispersion terms, respectively. Superscripts (vw) in the $E^{(vw)}$ terms define the order of V in $W_A + W_B$; the subscript ‘resp’ indicates that the orbital relaxations are included. The δ_{HF} term in the equation (number) is computed from the Hartree–Fock supermolecular interaction energy (E_{int}^{HF}). It takes into account higher order induction effects and is defined as:

$$\delta_{HF}^{(2)} = E_{int}^{(2)} - (E_{elst}^{(10)} + E_{exch}^{(10)} + E_{ind,resp}^{(20)} + E_{exch-ind}^{(20)}) \tag{8}$$

Intrinsic free energy of solvation corresponds to the change in Gibbs free energy of the solute (system under study) in the gas and solution phase [40].

$$\Delta G_s = G_{soln}(R_l) - G_{gas}(R_g) \tag{9}$$

and

$$\Delta G_s = E_{soln}(R_l) - E_{gas}(R_g) + G_{soln}^{corr}(R_l) - G_{gas}^{corr}(R_g) + G_{nes}(R_l) \tag{10}$$

$$E_{soln} = \left\langle \psi_{pol} \left| H^o + \frac{V}{2} \right| \psi_{pol} \right\rangle \tag{11}$$

where E_{soln} and E_{gas} are the solute electronic energy in the gas phase and solution phase, respectively. G^{corr} is the thermal correction factor to Gibbs free energy, G_{nes} is the non-electrostatic component of the solvation energy, ψ_{pol} is the wave function corresponding to polarized solute–solvent system, H^o is the Hamiltonian corresponding to unpolarized solute–solvent system, and v is the solute–solvent interaction parameter.

Dipole moment and polarizability are two important properties to characterize a piezoelectric material. The dipole moment is the first derivative of energy with respect to an applied electric field. It is the measure of the asymmetry in the molecular charge distribution and is given as a vector in three dimensions (X, Y, and Z) as μ_x , μ_y , and μ_z , respectively. Molecular polarizability is quantified as the second derivative of the energy of the molecule with respect to an electric field. Net dipole moments (μ_0) and mean polarizabilities (α_0) are calculated from the dipole moment vectors (μ_x , μ_y , μ_z) and molecular exact polarizability tensors (α_{xx} , α_{yy} , α_{zz}) according to the following mathematical formulae [41]:

$$\mu_0 = \left(\mu_x^2 + \mu_y^2 + \mu_z^2 \right)^{\frac{1}{2}} \quad (12)$$

$$\alpha_0 = \frac{1}{3} (\alpha_{xx} + \alpha_{yy} + \alpha_{zz}) \quad (13)$$

Frontier orbitals (highest occupied molecular orbital (HOMO) and lowest unoccupied molecular orbital (LUMO)) energies of a molecule can be directly correlated to different chemical parameters, which provide thorough insight to the reactivity and selectivity of it. According to Koopmans theorem [42] for close-shell Hartree–Fock calculations, ionization potential $IP = -HOMO$ energy and electron affinity $EA = -LUMO$ energy. Although Koopmans' theorem is mainly applicable for closed shell Hartree–Fock calculations, it also holds quite well for the long range corrected (LC) density functional [43]. The present calculations are all performed in dispersion corrected functional B3LYP-D where the rectifications regarding the long-range behavior is present [20]. Using finite approximation for the small change in the number of particles, different physical and chemical parameters can be evaluated from these HOMO- LUMO energy values [44, 45] as given below:

$$\text{Electronegativity } (\chi) = \frac{IP + EA}{2} \quad (14)$$

$$\text{Chemical potential } (\mu) = -\left(\frac{IP + EA}{2} \right) \quad (15)$$

$$\text{Chemical hardness } (\eta) = \frac{IP - EA}{2} \quad (16)$$

$$\text{Chemical softness } (S) = \frac{1}{\eta} \quad (17)$$

$$\text{Electrophilicity index } (\omega) = \left(\frac{\left(\frac{IP + EA}{2} \right)^2}{IP - EA} \right) = \frac{\mu^2}{2\eta} \quad (18)$$

Intra- and inter-unit energetic interactions within the systems under study are characterized by natural bond orbital (NBO) analysis [23], carried out by the NBO 3.1 program implemented in the Gaussian09 package, which quantifies the loss of electron density (electron delocalization) from the donor (Lewis) NBOs into empty acceptor (non-Lewis) NBOs during interaction, resulting in significant departure from the idealized Lewis structures. The extent of electron delocalization is proportional to the stabilization energy ($E^{(2)}$) associated with i (donor) $\rightarrow j$ (acceptor) delocalization and is mathematically defined using the second order perturbation theory as follows:

$$E^{(2)} = \Delta E_{ij}^{(2)} = \frac{q_i F(i, j)^2}{\epsilon_j - \epsilon_i} \quad (19)$$

where q_i is donor orbital occupancy, ϵ_i and ϵ_j are diagonal elements of the Fock matrix, and $F(i, j)$ are the off-diagonal

elements of the Fock matrix.

In order to get further insight into the nonbonding interaction, topological analysis is carried out in accordance with Bader's quantum theory of atoms in molecules (QTAIM) analysis [24] using Multifunctional Wavefunction Analyser (Multiwfn) [46] at B3LYP-D/6-311+G(d,p) computation level. Electron density (ρ) and Laplacian of electron density ($\nabla^2\rho$) are obtained at the bond critical points (BCPs, where $\nabla\rho = 0$) corresponding to relatively higher inter-unit NBO interaction regions. Positive values of $\nabla^2\rho$ and reasonably small ρ values verify the noncovalent interactions within complex molecules. More detailed topological information is attained on the basis of the Virial theorem relating the topological parameters and Laplacian of electron density at the BCPs, as:

$$\frac{1}{4} \nabla^2\rho = 2G + V \quad (20)$$

$$H = G + V \quad (21)$$

where G , V , and H are the kinetic, potential, and total energy densities at the critical point, respectively. The condition for noncovalent interaction is: $\frac{G}{|V|} > 1$.

Another parameter that determines the binding strength of an atom pair (bonded or nonbonded) is the delocalization index (DI) 'δ' [25], which is derived from domain-averaged exchange-correlation energy and provides a quantitative measure of the number of electron pairs delocalized (or shared) between two atomic spaces. For α electrons, DI is mathematically formulated as:

$$\delta^\alpha(A, B) = -2 \int_A \int_B \Gamma_{XC}^{\alpha, \text{tot}}(r_1, r_2) dr_1 dr_2 \quad (22)$$

where A, B refer to the atom pair, and Γ_{XC} is the exchange-correlation density. For β electrons, the α in the equation (number) is to be replaced by β . In the present work, DI values are calculated in the fuzzy atomic space [47] using the Multiwfn program [46].

Inter-unit Hirshfeld surface analysis [26, 48] is performed using Multifunctional Wavefunction Analyser (Multiwfn) [46]. The Hirshfeld surface well explains the inter molecular interactions and it is based on the concept of the Hirshfeld weight function of an atom, which is expressed as:

$$w_A^{\text{Hirsh}}(r) = \frac{\rho_A^0(r)}{\sum_B \rho_B^0(r)} \quad (23)$$

where ρ_A^0 denotes the density of atom 'A' in free space. Overall Hirshfeld weight of a particular unit (or fragment) 'P' of a complex molecule is the summation of weight of all the atoms within the unit, i.e.,

$$w_P^{\text{Hirsh}}(r) = \sum_{A \in P} w_A^{\text{Hirsh}}(r) \quad (24)$$

Hirshfeld surface of a fragment ‘P’ is the isosurface corresponding to $w_p^{\text{Hirsh}} = 0.5$. Large electron density values in some local regions of the Hirshfeld surface infer higher inter-unit interaction corresponding to the regions within the complex system.

The Hirshfeld fingerprint plot [48] is very useful for investigating the noncovalent interactions in molecular crystals. X and Y axes in this plot correspond to d_i and d_e , respectively, d_i (and d_e) being the distance from a point on the surface to the nearest nucleus inside (and outside) the surface. The standard 0.6–2.6 Å range is set for both d_i and d_e . The plot is created by binning (d_i, d_e) pairs in certain intervals and coloring each bin of the resulting 2D histogram as a function of the number of surface points in that bin, ranging from purple (few points) through green to red (many points). A black region means absence of surface points. Hirshfeld fingerprint plots, mapped onto promolecular electron density, are obtained from the Multiwfn [46] program using protein data bank (PDB) files as input to obtain the plots.

The noncovalent interaction (NCI) study on the basis of reduced density gradient (RDG) analysis [27] provides graphical visualization of the region where noncovalent interactions occur in real space. This analysis helps to identify noncovalent

interactions on the basis of a 2D plot of RDG (s) and the electron density ρ according to the following mathematical relation:

$$s = \frac{1}{2(3\pi^2)^{1/3}} \frac{|\nabla\rho|}{\rho^{4/3}} \quad (25)$$

In this method, hydrogen bonds, van der Waals interactions, and repulsive steric interactions can be distinguished in terms of RDG ‘s’ vs ‘sign $(\lambda_2)\rho$ ’ plot, where sign $(\lambda_2)\rho$ is the electron density (ρ) multiplied by the sign of the second Hessian eigen value (λ_2). For a repulsive interaction, sign $(\lambda_2)\rho > 0$ and for attractive interaction, sign $(\lambda_2)\rho < 0$. Stronger attractive interactions show peaks at higher density values ($\rho > 0.01$), whereas peaks appearing at lower density values ($\rho < 0.01$; regions at the vicinity of the origin of the RDG plot) correspond to weaker van der Waals interactions. Inter-unit interactions in the NCI method can be visualized by gradient isosurface in real space. The color code for the visualization of the NCI isosurface is: blue for relatively strong attractive (hydrogen bonding), red for repulsive, and green for weak attractive (van der Waals) interactions. In

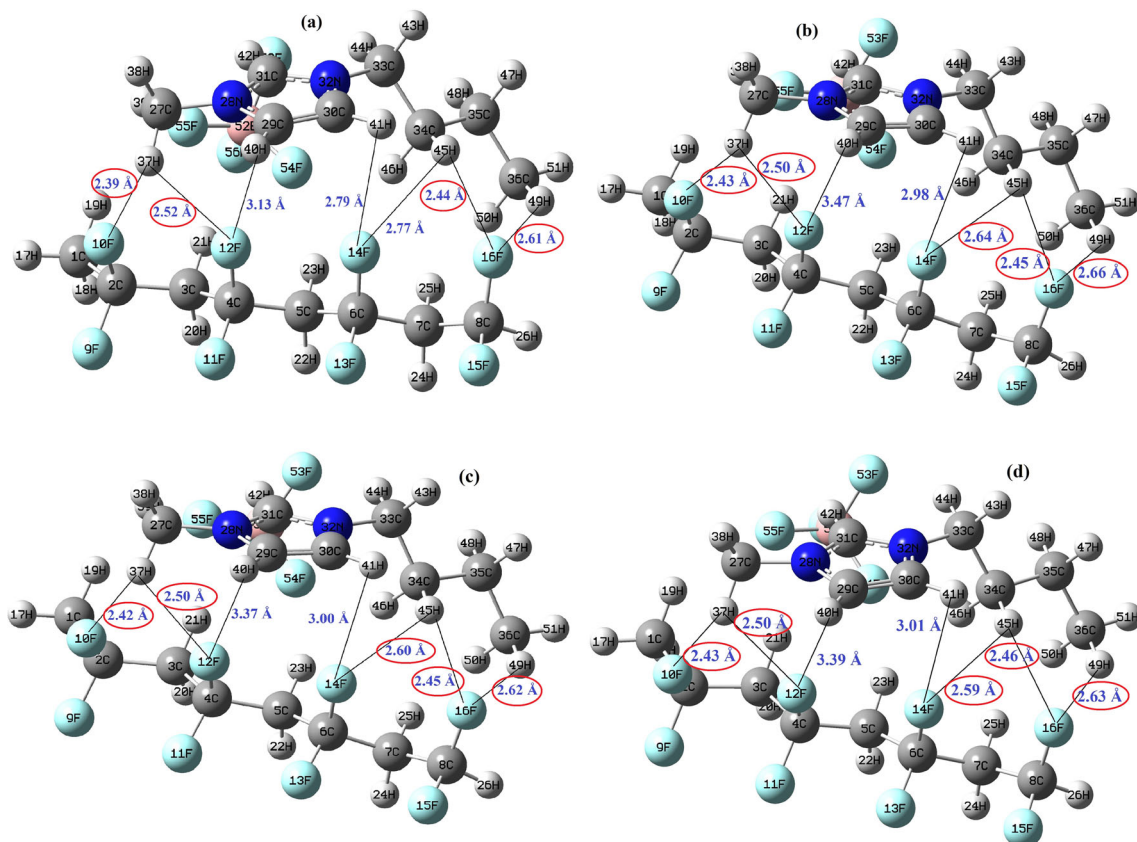


Fig. 1 Optimized structure of β -PVDF/[BMIM][BF₄] showing [BMIM]⁺/ β -PVDF average distances **a** in gas phase, **b** solvated with THF, **c** solvated with acetone, **d** solvated with DMF. [Simulation method: B3LYP-D/6–311+G(d,p)]. C–H···F bond lengths are marked as red ellipses

the current study, NCIPLOT-3.0 [27] and the visual molecular dynamics (VMD) program [49] are used for RDG analysis and gradient isosurface plot of the systems under study. SCF calculations using the wave function information are performed to obtain gradient isosurface visualization; $\rho = 0.05$ and $s = 2$ are used as cut off values.

Gaussian09 calculates standard thermodynamic parameters, e.g., standard enthalpy, heat capacity, and entropy resulting from translational, rotational, and vibrational motion of a system by a statistical thermodynamics approach. All the calculations start from partition function $q(V, T)$ for the corresponding component of the total partition function [50]. Temperature dependence of thermal correction factors to total energy (E_{corr}), enthalpy (H_{corr}), and Gibbs free energy (G_{corr}) are calculated using the freqcheck utility of the Gaussian09 program. Mathematical formulations of temperature dependence of standard thermodynamic parameters, e.g., absolute entropy, heat capacity at constant pressure, and enthalpy gradient are obtained with the help of Perl code thermo.pl [51].

Results and discussions

Geometry optimization

Optimized structures of β -PVDF/[BMIM][BF₄] complex in gas phase and solution phase with three different solvents, namely THF, acetone, and DMF, showing IL cation ([BMIM]⁺)/ β -PVDF and IL anion ([BF₄]⁻)/ β -PVDF inter unit distances, are presented in Figs. 1 and 2, respectively. Gas phase geometries of isolated α -PVDF, β -PVDF (both C_s and C₁ symmetry), and [BMIM][BF₄] are given in supplementary Fig. S2. Detailed descriptions of structural parameters of isolated PVDF, IL, and PVDF/IL complexes in gas and solution phases are provided in Table 1 and supplementary Tables S1 and S2. The zero point error (ZPE) corrected total energy (E_0) values of isolated α - and β -PVDF (as given in Table 2) suggest higher stability (lower E_0) of α -PVDF having trans-gauche configuration (TGTG') than β -PVDF possessing all-trans (TTTT) configuration. According to a previous study [53], the all-trans β -PVDF structure is

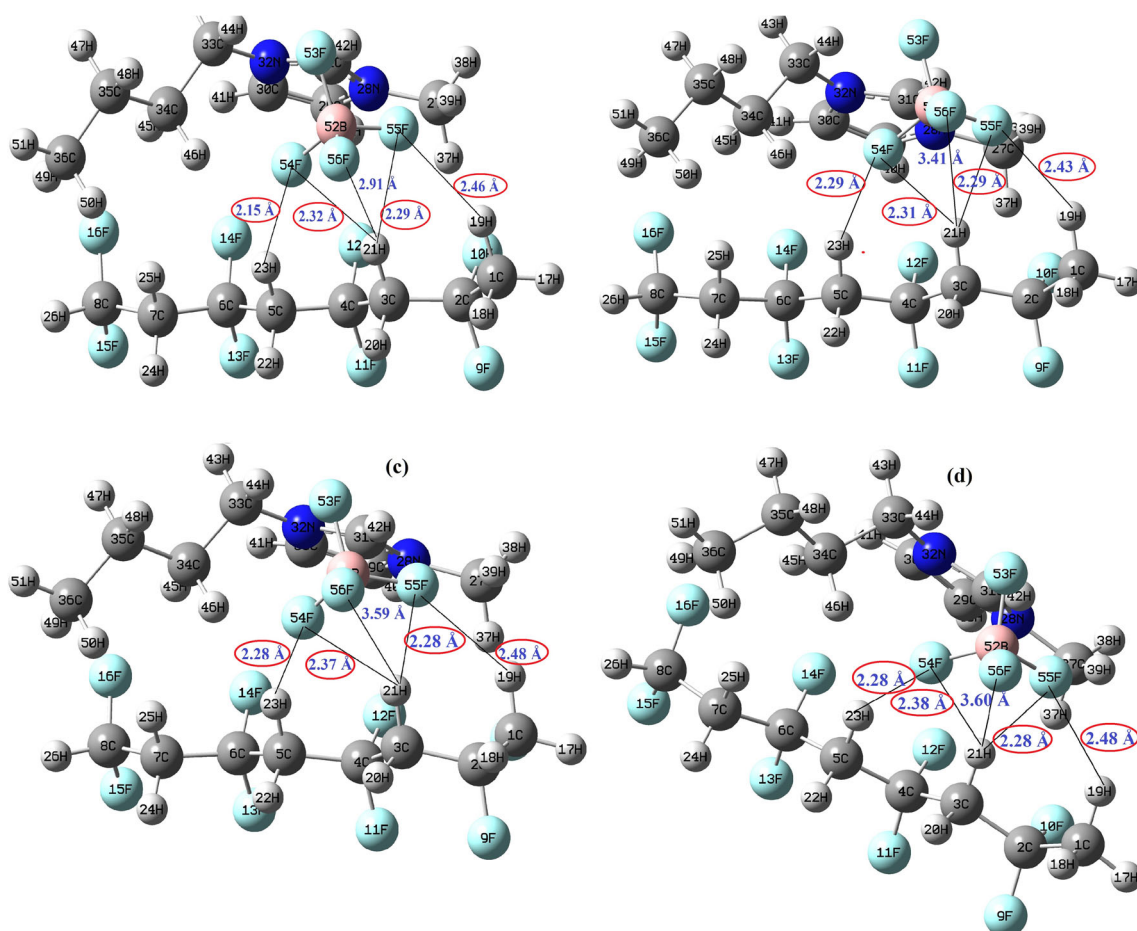


Fig. 2 Optimized structure of β -PVDF/[BMIM][BF₄] showing [BF₄]⁻/ β -PVDF average distances **a** in gas phase, **b** solvated with THF, **c** solvated with acetone, **d** solvated with DMF. [Simulation method: B3LYP-D/6-311+G(d,p)]. C–H...F bond lengths are marked as red ellipses

Table 1 Average values of structural parameters of β -PVDF before and after ionic liquid addition in gas phase and solvated phase. Simulation method: B3LYP-D/6-311+G(d,p). [Available experimental [52] results are given within {} brackets]

Structural parameters ^a	Isolated state				Complex state				
	Gas phase	In THF	In acetone	In DMF	Gas phase	In THF	In acetone	In DMF	
Bond length (Å)	d_{C-F}	1.372 {1.34}	1.380	1.380	1.382	1.378	1.382	1.383	1.383
	d_{C-H}	1.093 {1.09}	1.092	1.092	1.092	1.092	1.089	1.091	1.091
	d_{C-C}	1.526 {1.54}	1.523	1.522	1.522	1.522	1.520	1.520	1.520
Bond angle ($^\circ$)	$\angle_{C_F-C_H-C_F}$	116.74 {112.5}	116.97	117.08	117.10	117.84	117.66	117.88	117.49
	$\angle_{C_H-C_F-C_H}$	111.88 {112.5}	112.14	112.17	112.18	111.16	111.58	110.75	111.78
	\angle_{F-C-F}	106.65 {108}	105.83	105.61	105.55	106.09	105.57	105.44	105.90
	\angle_{H-C-H}	108.51 {112}	108.18	108.11	108.09	108.64	108.15	107.69	107.89
Dihedral angle ($^\circ$)	$C-C-C-C$	167.24	167.24	167.84	167.95	172.86	172.31	170.06	169.74

^a Structural parameters: d_{C-C} , d_{C-F} , d_{C-H} are the average distances between two adjacent C atoms present in the PVDF backbone, C and F atoms within a CF_2 group, and C and H atoms within a CH_2 group, respectively; $\angle_{C_F-C_H-C_F}$ and $\angle_{C_H-C_F-C_H}$ are the angle between two adjacent C-C bonds, C_F represents the C atoms bonding with two F atoms, and C_H refers to the C atoms bonding with two H atoms, \angle_{F-C-F} , \angle_{H-C-H} are the angle between two C-F bonds, and two C-H bonds, respectively, $C-C-C-C$ is the dihedral angle constituted by four adjacent C atoms of the PVDF backbone chain

supposed to exhibit C_S symmetry, but optimized β -PVDF tetramer with C_S symmetry results in three imaginary frequencies inferring the instability of the molecule. Therefore, the β -PVDF structure is re-optimized keeping the point group symmetry restricted as C_1 and then all the frequencies are found as positive. However, the E_0 value of β -PVDF (with C_1 symmetry) is still found to be larger than that of α -PVDF further confirming higher stability of isolated α -PVDF with respect to β -PVDF (refer Table 2). However, the β -PVDF fragment within the β -PVDF/IL complex exhibits C_1 symmetry. Average values of bond length, bond angle, and dihedral angle of the β -PVDF molecule within pure state and complex state (with [BMIM][BF₄]) in gas and solution states are given in Table 1. The inter-fragment distances of β -PVDF/[BMIM][BF₄] complex, as shown in Figs. 1 and 2, indicate probable sites of inter-unit hydrogen bond interactions between fluorine atoms of PVDF and hydrogen atoms of [BMIM]⁺ cation, and the hydrogen atoms of PVDF and fluorine atoms of [BF₄]⁻ anion. According to the characteristics of hydrogen bonds, the hydrogen bond length should be shorter than the sum of the van der Waals (vdW) radii of the hydrogen atom and the other atom forming the bond [54]. Therefore, H \cdots F bond length should be less than 2.67 Å (as the vdW radii of hydrogen and fluorine atoms are 1.2 Å and 1.47 Å, respectively [54, 55]). The inter-unit H \cdots F bonds corresponding to [BMIM]⁺/ β -PVDF and [BF₄]⁻/ β -PVDF interactions are marked as red ellipses in Figs. 1 and 2, respectively. Although intra-unit structural parameters are not found to vary much, considerable variations in the inter-unit H \cdots F distances are observed for PVDF/IL complexes after solvation. For example, an additional H \cdots F bond is found between 14F (within PVDF) and 45H (within [BMIM]⁺) in the solution phase but the distance between these two atoms in the gas phase is 2.77 Å, which is beyond the range of H \cdots F hydrogen bond

distance (refer Fig. 1). In the case of both gas phase and solution phase calculations, the dipole moment of the β -PVDF/IL complex is obtained as less than the individual β -PVDF and IL molecule as given in Table 2, which suggests better ion-dipole interactions occurring among the constituting units of the complex systems. However, mean dipole moment values (μ_0) of all the systems increase significantly after solvation, and the amount of increment is found to be directly proportional to solvent polarity. This results from the additional dipole moment induced by the reaction field of the solvent continuum [23]. Polarizability values (α_0) are also calculated and given in Table 2, which shows direct proportionality of the polarizability values to the size of the system. The β -PVDF/IL complex possesses the highest polarizability value and the β -PVDF molecule is associated with the least polarizability, whereas ionic liquid [BMIM][BF₄] shows intermediate value of polarizability. The polarizability values of the systems also increase upon solvation. However, the trend of the change in polarizability upon complexation is found to be similar for both gas and solvation model calculations.

Energy calculations

The energy values associated with the optimized structures of α -PVDF, β -PVDF, and β -PVDF/[BMIM][BF₄] in the gas phase and solution phase are given in Table 2. The isolated β -PVDF molecule possesses higher E_0 than α -PVDF, but β -PVDF/[BMIM][BF₄] exhibits lower E_0 than α -PVDF/[BMIM][BF₄]. This fact indicates stabilization of the less stable β -PVDF system after ionic liquid addition. However, the energy values of all the systems become more negative within polar solvent continuum (the higher the solvent polarity, the lower the energy). Energy (E_0) differences for isolated α - and β -PVDF conformers ($\Delta E_{\beta-\alpha} = E_{\beta} - E_{\alpha}$) are found to be

Table 2 ZPE corrected energy (E_0), solvation free energy (ΔG_s), dipole moment (μ_0), polarizability (α_0), basis set superposition error (BSSE), binding energy (ΔE_b), and supermolecular interaction energy (ΔE_i) of the systems. [Simulation method: B3LYP-D/6-311+G(d,p); solvent model: IEFPCM]

Systems	Parameters	Gas phase	In THF	In acetone	In DMF
α -PVDF	E_0 (a.u)	-1109.844	-1109.856	-1109.858	-1109.858
	ΔG_s (kcal mol ⁻¹)	-	-7.40	-8.78	-9.17
	μ_0 (D)	4.95	6.28	6.59	6.68
	α_0 (a.u)	97.852	116.034	119.612	120.639
β -PVDF	E_0 (a.u)	-1109.830	-1109.849	-1109.853	-1109.854
	ΔG_s (kcal mol ⁻¹)	-	-12.11	-14.82	-15.35
	μ_0 (D)	7.81	10.24	10.80	10.96
	α_0 (a.u)	99.527	116.744	120.158	121.151
[BMIM][BF ₄]	E_0 (a.u)	-847.902	-847.928	-847.933	-847.934
	ΔG_s (kcal mol ⁻¹)	-	-17.63	-20.78	-21.71
	BSSE (kcal mol ⁻¹)	1.77	-	-	-
	μ_0 (D)	10.8032	13.9587	14.5256	14.7114
α -PVDF/[BMIM][BF ₄]	E_0 (a.u)	-1957.762	-1957.797	-1957.803	-1957.805
	ΔG_s (kcal mol ⁻¹)	-	-22.97	-26.93	-28.07
	ΔE_b (kcal mol ⁻¹)	-11.16	-9.16	-9.24	-9.13
	ΔE_i (kcal mol ⁻¹)	-11.61	-9.11	-9.70	-9.53
β -PVDF/[BMIM][BF ₄]	E_0 (a.u)	-1957.775	-1957.803	-1957.808	-1957.809
	ΔG_s (kcal mol ⁻¹)	-	-18.75	-22.59	-23.63
	ΔE_b (kcal mol ⁻¹)	-27.67	-16.78	-14.83	-14.28
	ΔE_i (kcal mol ⁻¹)	-31.42	-18.23	-15.92	-15.31
	BSSE (kcal mol ⁻¹)	4.37	-	-	-
	μ_0 (D)	5.8673	8.0804	8.6417	8.7471
	α_0 (a.u)	219.823	266.797	276.044	278.794

8.78 kcal mol⁻¹ in gas phase, 4.39 kcal mol⁻¹ in THF, 3.13 kcal mol⁻¹ in acetone, and 2.51 kcal mol⁻¹ in DMF; and for PVDF/IL complexes, energy differences ($\Delta E_{\alpha\text{PVDF/IL}} - \beta\text{PVDF/IL} = E_{\alpha\text{PVDF/IL}} - E_{\beta\text{PVDF/IL}}$) are 8.16 kcal mol⁻¹ in gas phase, 3.67 kcal mol⁻¹ in THF, 3.14 kcal mol⁻¹ in acetone, and 2.51 kcal mol⁻¹ in DMF. For both cases, energy difference values are found to decrease with increasing solvent polarity.

Solvation free energies (ΔG_s) of isolated and complex systems are listed in Table 2. All the systems discussed here possess negative solvation free energy, i.e., perfect solubility within polar solvents. Notably, solvation free energy becomes more negative with solvent polarity, as shown in Table 2. Binding energy values (ΔE_b) of PVDF/IL complexes suggest better binding of ionic liquids with β -PVDF than with α -PVDF. BSSE corrected supermolecular interaction energy (ΔE_i) values are obtained for PVDF/IL systems. [BMIM][BF₄] possesses negative interaction energy with both α - and β -PVDF, but the magnitude is higher (more negative) in the case of β -PVDF/IL complex in gas phase, as well as solution phases. This can be a suitable implication of the increase in fractional content of electroactive β -PVDF crystals

in the PVDF blend after ionic liquid addition. Significant reduction (less negative) in ΔE_b and ΔE_i values are observed in the case of solvation model calculations. This fact is attributed to the separate interaction between the solvent continuum and the constituting units (β -PVDF, [BMIM]⁺, [BF₄]⁻) of the complex [56]. However, as shown in Table 2, the highest magnitudes of ΔE_b and ΔE_i are found within acetone. Perturbative treatment of inter-fragment interactions within PVDF/IL complexes is performed using SAPT analysis considering two fragments; fragment 1 and 2 being the PVDF and IL parts respectively, each possessing neutral charge and singlet multiplicity. SAPT0 and SAPT2 energy values are calculated for α -PVDF/IL and β -PVDF/IL systems using their optimized geometries in the gas and solution phases and provided in Table 3. Although SAPT does not account for the solvent effect, calculations are performed for solution phase equilibrium structures also, to clarify the structure-dependent dispersion contribution to the total interaction energy. However, magnitudes of the total SAPT energies (SAPT0 and SAPT2) and their components are also found to be lower in the case of α -PVDF/IL than β -PVDF/IL. Although the attractive

Table 3 SAPT0 and SAPT2 interaction energies of (α and β -) PVDF/IL complex systems

SAPT energy components	SAPT0 [SAPT2] calculation on gas phase geometry of PVDF/[BMIM][BF ₄]		SAPT0 [SAPT2] calculation on solution phase (in THF) geometry of PVDF/ [BMIM][BF ₄]		SAPT0 [SAPT2] calculation on solution phase (in acetone) geometry of PVDF/[BMIM][BF ₄]		SAPT0 [SAPT2] calculation on solution phase (in DMF) geometry of PVDF/ [BMIM][BF ₄]	
	α -PVDF/IL	β -PVDF/IL	α -PVDF/IL	β -PVDF/IL	α -PVDF/IL	β -PVDF/IL	α -PVDF/IL	β -PVDF/IL
Electrostatic (kcal mol ⁻¹)	-7.091 [-8.028]	-26.198 [-26.258]	-8.381 [-8.467]	-25.647 [-25.678]	-9.067 [-9.385]	-24.609 [-24.852]	-9.073 [-9.398]	-24.471 [-24.710]
Exchange (kcal mol ⁻¹)	9.181 [10.697]	23.940 [27.557]	9.441 [10.951]	21.806 [25.217]	11.629 [13.611]	21.674 [21.674]	11.677 [13.665]	21.416 [21.824]
Induction (kcal mol ⁻¹)	-1.716 [1.889]	-6.534 [-7.043]	-1.861 [-2.039]	-6.451 [-6.971]	-1.910 [-2.104]	-6.411 [-6.919]	-1.916 [-2.111]	-6.377 [-6.882]
Dispersion (kcal mol ⁻¹)	-6.664 [-5.890]	-13.736 [-13.750]	-6.598 [-6.604]	-13.510 [-13.522]	-8.049 [-8.056]	-13.627 [-13.640]	-8.068 [-8.074]	-13.560 [-13.573]
Total (kcal mol ⁻¹)	-7.101 [-5.890]	-22.527 [-19.494]	-7.340 [-6.158]	-23.808 [-20.954]	-7.397 [-5.934]	-22.974 [-20.305]	-7.380 [-5.919]	-22.991 [-20.341]

interaction is majorly electrostatic (~70%), a significantly large value of dispersion energy (~30%) infers the presence of long range interactions acting between PVDF and IL fragments.

IR spectroscopy analysis

Vibrational frequency analysis is performed using a frequency scaling factor of 0.9877, which is consistent with the present level of theory [57]. Simulated IR spectra of isolated α - and β -PVDF (four monomer units), ionic liquid [BMIM][BF₄], and β -PVDF/[BMIM][BF₄] in the gas phase, within the frequency range of 500–3500 cm⁻¹ are presented in Fig. 3 and compared with experimental findings. [Complete IR spectra of the systems in the solution phases are given in supplementary Fig. S3]. IR data of α - and β -PVDF have shown excellent agreement with the same analyses reported by Wang et al. [53], supporting the reliability of the present calculation scheme (B3LYP-D/6-311+G(d,p)). According to vibrational assignments, complete IR spectra of isolated α - and β -PVDF are divided into five (I, II, III, IV, and V) frequency bands, such as, band I (>3000 cm⁻¹), band II (1435–1470 cm⁻¹), band III (1125–1420 cm⁻¹), band IV (750–1130 cm⁻¹), and band V (400–700 cm⁻¹). Band I corresponds to C–H stretching frequencies for both of α - and β -PVDF. For α -PVDF, band II corresponds to in-plane bending of –CH₂ groups, band III mainly results from the strong out-of-plane bending of C–H bonds of –CH₂ units and weak torsional movement of polymer backbone chain, and band IV and V are formed owing to –CF₂ and –CH₂ rocking and in-plane bending of polymer backbone chain. In the case of β -PVDF, the highest IR intensity is observed in band III at 1263 cm⁻¹ (corresponds to the symmetrical perpendicular movement of the carbon atoms, attached to the fluorine atoms, with respect to the polymer backbone) and 1221 cm⁻¹ (corresponds to –CH₂ twisting and C–F

bond stretching). Some characteristic peaks of β -PVDF are observed in band IV at the frequencies 749, 807, and 826 cm⁻¹, which result from the asymmetric in-plane movement of –CH₂ groups, perpendicular to polymer chain. In band V, some important peaks are observed at 443 cm⁻¹

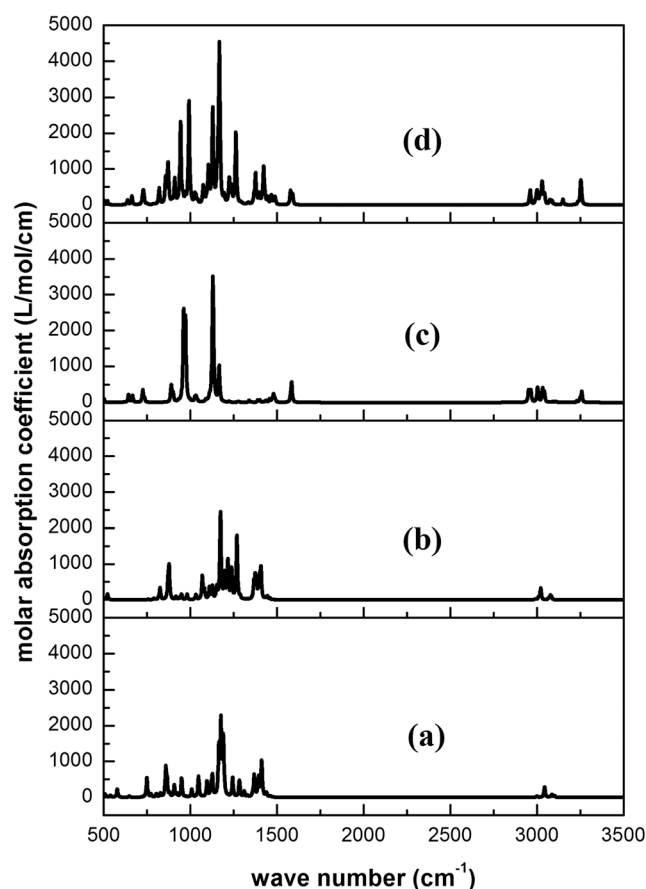


Fig. 3 Complete IR spectra (simulated) of (a) α -PVDF, (b) β -PVDF, (c) [BMIM][BF₄], and (d) β -PVDF/[BMIM][BF₄] in the gas phase. [Simulation method: B3LYP-D/6-311+G(d,p)]

Table 4 C–H stretching vibration modes of simulated IR spectra in gas phase DFT model and solvation DFT model. [ν_{sym} and ν_{asym} refer to the symmetrical and asymmetrical stretching, respectively. The numbers within the {} brackets correspond to the peak positions shown in Fig. 4] [red shifting frequencies are marked as bold]

(a) Pure β -PVDF			Solvation model calculations (IEFCM)			Assignment	Experimental values [61] Frequency (cm^{-1})
Mode	Gas phase calculations Frequency (cm^{-1})	Assignment	In THF	In acetone	In DMF		
63	2990.13 {1}	ν_{sym} (terminal CH_3)	2993.59 {1}	2994.41 {1}	2994.68 {1}	ν_{sym} (terminal CH_3)	2980
64	3008.29	ν_{sym}	3021.94	3024.41	3025.07	ν_{sym}	
65	3012.92	ν_{sym}	3023.63	3052.87	3026.72	ν_{sym}	
66	3018.25	ν_{sym}	3030.02 {2}	3032.15 {2}	3032.70 {2}	ν_{sym}	
67	3022.30 {2}	ν_{sym}	3054.85 {3}	3061.12 {3}	3062.82 {3}	ν_{sym}	
68	3.62.91	ν_{asym}	3074.20	3075.95	3076.62	ν_{asym}	3022
69	3066.33	ν_{asym}	3075.66	3077.32	3077.97	ν_{asym}	
70	3071.05	ν_{asym}	3081.75	3083.91	3084.37	ν_{asym}	
71	3077.90 {3}	ν_{asym} (terminal CH_3)	3084.47 {4}	3085.36 {4}	3085.53 {4}	ν_{asym} (terminal CH_3)	
72	3084.52	ν_{asym}	3086.48	3087.10	3087.46	ν_{asym}	
(b) [BMIM][BF ₄] [red shifting frequencies are marked as bold]			Solvation model calculations (IEFPCM)			Assignment	Experimental values [62] Frequency (cm^{-1})
Mode	Gas phase calculations Frequency (cm^{-1})	Assignment	In THF	In acetone	In DMF		
70	2951.52 {1}	ν_{sym} (butyl)	2957.17	2956.80	2956.50	ν_{sym} (butyl)	2878
71	2959.87	ν_{sym} (butyl)	2957.95 {1}	2958.48 {1}	2958.75 {1}	ν_{sym} (butyl)	
72	2965.15 {2}	ν_{asym} (butyl)	2979.33 {2}	2981.47 {2}	2982.14 {2}	ν_{asym} (butyl)	2942
73	3002.39	ν_{asym} (butyl)	2995.67 {3}	2995.08 {3}	2994.97 {3}	ν_{asym} (butyl)	
74	3003.22 {3}	ν_{asym} (butyl)	3010.29 {4}	3013.81 {4}	3014.19 {4}	ν_{asym} (butyl) + ν_{sym} (butyl) (low)	
75	3007.63	ν_{asym} (methyl)	3014.32	3014.38	3014.87	ν_{asym} (butyl)	2966
76	3033.08 {4}	ν_{asym} (butyl)	3029.46 {5}	3028.18 {5}	3027.73 {5}	ν_{asym} (butyl)	
77	3042.92	ν_{asym} (butyl)	3035.26	3033.77	3033.41	ν_{asym} (butyl)	
78	3072.83	ν_{asym} (butyl)	3062.25 {6}	3059.25 {6}	3058.49 {6}	ν_{asym} (butyl)	
79	3091.14 {5}	ν_{asym} (butyl)	3088.90 {7}	3088.77 {7}	3088.71 {7}	ν_{asym} (butyl)	3105
80	3102.09	ν_{asym} (methyl)	3107.69	3106.74	3106.38	ν_{asym} (methyl)	
81	3111.99 {6}	ν_{asym} (methyl)	3115.49 {8}	3116.40 {8}	3116.58 {8}	ν_{asym} (methyl)	
82	3231.4 {7}	ν_{asym} (imida-zolium ring)	3233.92 {9}	3234.63 {9}	3234.82 {9}	ν_{asym} (imida-zolium ring)	3123
83	3249.68	ν_{asym} (imida-zolium ring)	3251.49 {10}	3251.98 {10}	3252.19 {10}	ν_{asym} (imida-zolium ring)	
84	3258.6 {8}	ν_{sym} (imida-zolium ring)	3267.57 {11}	3268.28 {11}	3268.60 {11}	ν_{sym} (imida-zolium ring)	3163
(c) β -PVDF/[BMIM][BF ₄] [red shifting frequencies are marked as bold]			Solvation model calculations			Assignment	Experimental values [62] Frequency (cm^{-1})
Mode	Gas phase calculations Frequency (cm^{-1})	Assignment	In THF	In acetone	In DMF		
138	2957.144	ν_{sym} (butyl, IL)	2957.79	2959.58	2959.47	ν_{sym} (IL, butyl)	
139	2961.618 {1}	ν_{sym} (butyl, IL)	2963.54 {1}	2963.25 {1}	2963.04 {1}	ν_{sym} (IL, butyl)	
140	2990.361	ν_{sym} (terminal CH_3 , PVDF)	2993.64	2994.31	2994.37	ν_{sym} (terminal CH_3 , PVDF)	
141	2997.452	ν_{sym} + ν_{asym} (butyl, IL)	2999.02 {2}	2998.38 {2}	2998.12 {2}	ν_{asym} (butyl, IL)	
142	2999.279 {2}	ν_{asym} (butyl, IL)	3013.41 {3}	3013.08 {3}	3013.36 {3}	ν_{sym} (methyl, IL)	
143	3002.618	ν_{asym} (methyl, IL)	3014.24	3013.82	3014.38	ν_{sym} (butyl, IL)	
144	3014.816	ν_{sym} (PVDF)	3024.38	3023.84 {4}	3024.77 {4}	ν_{sym} (butyl, IL)	
145	3017.848	ν_{sym} (butyl, IL)	3030.37 {4}	3030.11	3029.99	ν_{sym} (butyl, IL) + ν_{sym} (PVDF) (low)	
146	3023.004	ν_{sym} (PVDF)	3030.67	3032.02	3032.17	ν_{asym} (butyl, IL) + ν_{sym} (PVDF) (low)	
147	3028.466	ν_{sym} (PVDF)	3036.47	3037.32	3037.56	ν_{sym} (PVDF)	
148	3030.718 {3}	ν_{asym} (butyl, IL)	3040.92 {5}	3041.46 {5}	3041.19 {5}	ν_{asym} (butyl, IL)	

Table 4 (continued)

149	3037.533	ν_{sym} (PVDF)	3042.62	3043.92	3043.88	ν_{sym} (PVDF)
150	3044.161 {4}	ν_{asym} (butyl, IL)	3054.71 {6}	3057.73 {6}	3059.27 {6}	ν_{sym} (PVDF)
151	3072.379	ν_{asym} (PVDF) + ν_{asym} (butyl, IL) (low)	3075.29 {7}	3069.49 {7}	3069.73 {7}	ν_{asym} (PVDF) + ν_{asym} (butyl, IL) (low)
152	3072.824	ν_{asym} (PVDF)	3080.09	3080.09 {8}	3080.22 {8}	ν_{asym} (terminal CH ₃ , PVDF)
153	3076.636 {5}	ν_{asym} (PVDF)	3085.68	3086.08	3086	ν_{asym} (PVDF)
154	3086.464	ν_{asym} (PVDF) + ν_{asym} (butyl, IL) (low)	3094.36	3094.37	3094.26	ν_{asym} (PVDF)
155	3087.698 {6}	ν_{asym} (butyl, IL) + ν_{asym} (PVDF) (low)	2998.87	3096.96	3097.5	ν_{asym} (butyl, IL) + ν_{asym} (PVDF) (low)
156	3090.671	ν_{asym} (terminal CH ₃ , PVDF)	3101.85	3101.78	3101.46	ν_{asym} (PVDF) + ν_{asym} (butyl, IL) (low)
157	3099.995	ν_{asym} (methyl, IL)	3105.48	3104.41	3104.78	ν_{asym} (methyl, IL)
158	3127.335	ν_{asym} (PVDF)	3123.11	3117.85 {9}	3117.17 {9}	ν_{asym} (PVDF)
159	3150.22 {7}	ν_{asym} (PVDF)	3124.89 {8}	3124.89	3125.29	ν_{asym} (methyl, IL)
160	3237.365 {8}	ν_{asym} (imidazolium ring)	3237.50 {9}	3237.50 {10}	3236.05 {10}	ν_{asym} (imidazolium ring)
161	3253.158 {9}	ν_{asym} (imidazolium ring)	3254.60 {10}	3254.60	3253.35	ν_{asym} (imidazolium ring)
162	3258.077	ν_{sym} (imidazolium ring)	3275.90 {12}	3275.90 {11}	3281.14	ν_{sym} (imidazolium ring)

(caused by $-\text{CF}_2$ and $-\text{CH}_2$ rocking), 480 cm^{-1} (corresponds to $-\text{CF}_2$ scissoring and $-\text{CH}_2$ moving perpendicular to the polymer chain) and 518 cm^{-1} (results from $-\text{CF}_2$ scissoring and in plane movement of $-\text{CH}_2$ groups), which also match with the previously reported results [53, 58].

In the IR spectrum of the isolated ionic liquid [BMIM][BF₄] system (refer to Fig. 3c), the frequency range $2960\text{--}3120\text{ cm}^{-1}$ (experimentally, $2800\text{--}3000\text{ cm}^{-1}$ [59]) corresponds to the stretching of the C–H bonds present in the methyl chain attached to 33 N atom and alkyl chain attached to 35 N atom. Some characteristic peaks within this range match consistently with experimental observations [59] (given within brackets), e.g., 2952 cm^{-1} (2856 cm^{-1}), 2960 cm^{-1} (2877 cm^{-1}), 2965 cm^{-1} (2913 cm^{-1}), and 3002.39 cm^{-1} (2965 cm^{-1}). Peaks corresponding to 3259 cm^{-1} (3163 cm^{-1}) and 3231 cm^{-1} (3122 cm^{-1}) result from symmetric and asymmetric stretching of C36–H42 and C37–H43 bonds, respectively. (Refer to Figs. 1 and 2 for atom numbers).

Figure 3d represents the IR spectrum of the β -PVDF/[BMIM][BF₄] system. Interestingly, the peak positions of the characteristic spectra of pure PVDF, as obtained from the experimental results reported by Shalu et al. [60], show good consistency with the simulated spectra of α -PVDF, which indicates higher fractional content of α -PVDF in pristine PVDF blend. For example, in the simulated IR spectrum of α -PVDF, asymmetric and symmetric stretching of the C–H bonds in the α -PVDF backbone chain appear within $3075\text{--}3103\text{ cm}^{-1}$ and $3000\text{--}3044\text{ cm}^{-1}$, respectively showing good consistence with the peaks found at 3026 cm^{-1} and 2985 cm^{-1} in the experimental IR spectrum of pristine PVDF the system. For β -PVDF/IL system, C–H asymmetric and symmetric stretching frequencies shift to frequency ranges $3077\text{--}3087\text{ cm}^{-1}$ and $3014\text{--}3028\text{ cm}^{-1}$, respectively, showing good agreement with experimental observations, as shown in Table 4.

Solvation effects on IR vibrational shifts and intensities are demonstrated for C–H stretching modes only and shown in Fig. 4(i)–(iii). Notably, for pure β -PVDF, all the C–H stretching frequencies show blue shift (i.e., increase in frequency) in solution phases with respect to the gas phase. On the other hand, in the case of pure ionic liquid [BMIM][BF₄] and PVDF/[BMIM][BF₄], some frequencies undergo red shift (marked as bold in Table 4) and some show blue shift in solution state. Red (or blue shift) of vibrational frequencies can be correlated to an increase (or decrease) in the C–H bond lengths of the systems after solvation [reference: supplementary Table S1]. In the present study, unlike the characteristic of a proper D–H (D = hydrogen bond donor) bond, the majority of the C–H stretching frequencies are found to undergo blue shift after solvation, leading to formation of so-called improper hydrogen bonds as discussed later in the “Weak interaction analysis” section. Significant changes in the IR intensities are

also observed in the solution phases with respect to the gas phase, although, IR spectra follow similar trends within the solvents. In Fig. 4, the sharp peaks in the C–H stretching part of the IR spectra are shown by numbers, and their descriptions are provided in Table 4 [peak numbers are given within {} brackets in the table]. Change in the intensities at C–H stretching vibrational modes, e.g., in Fig. 4 (ii), the peak at 3003.22 [marked as 3] in (a) decomposes into triplets marked as 2, 3, 4 in (b), (c), (d). These changes are attributed to the effect of the solvent continuum on the IR intensity as explained by Cammi et al. [63]. Solvation effects on IR intensities are separated in two terms, the first one is the change in the molecular charge density caused by the dielectric solvent continuum, and the second one is the polarization of the solvent dielectric caused by the externally applied electric field, after the cavity is formed.

Frontier molecular orbital analysis and calculation of chemical parameters

Frontier molecular orbitals (HOMO and LUMO) are very crucial as they determine the chemical reactivity of a system [demonstrated in Fig. 5]. Atoms associated with higher contribution to HOMO and LUMO distributions act as potential electron donors and acceptors, respectively. HOMO and LUMO distributions in pure β -PVDF, [BMIM][BF₄], and β -PVDF/[BMIM][BF₄] molecules, both in gas phase and solution phase, are represented in Figs. 6, 7, and 8. HOMO-LUMO compositions of the isolated β -PVDF molecule in gas and solution phases are provided in supplementary Table S3, which shows the carbon atoms in the polymer backbone chain and the fluorine atom pairs in the β -PVDF

molecule share almost equal contribution (ranging 4–8% by each C and F atom) to HOMO. LUMO majorly consists of C and H atoms present in the molecule. As evident from Figs. 7 and 8, in the case of isolated IL and as well as β -PVDF/IL complex, the carbon and the nitrogen atoms in the imidazolium ring contribute to the highest portion of total HOMO and LUMO distributions. Atoms within the β -PVDF/[BMIM][BF₄] system with the highest HOMO and LUMO contributions are shown in supplementary Tables S4 and S5, respectively.

Different chemical parameters of the systems are obtained from HOMO-LUMO energies using Eqs. 14–18 and provided in Table 5. It is worth mentioning that Koopman's theorem is based on the Hartree–Fock method and does not hold for usual density functionals because of the exchange-correlation potential term present in the Hamiltonian [43]. In the case of long range corrected density functionals (like B3LYP-D) the exchange correlation term is presumed to be zero, and therefore they produce almost correct values of IP and EA as compared to the usual density functionals. For comparison, single point energy calculations are performed using the Hartree–Fock method and 6–311+G(d,p) basis set, on the structures as optimized using the B3LYP-D functional and the same basis set. The chemical parameters are calculated according to Eqs. 14–18 using the HOMO-LUMO energy values obtained from both HF and B3LYP-D simulations, in the gas and solution phases, and the comparison is shown in Fig. 5. Solvation produces notable variation in the HOMO-LUMO energy levels, thereby changing the chemical parameters but the pattern of this change is found to be almost similar for both the aforementioned

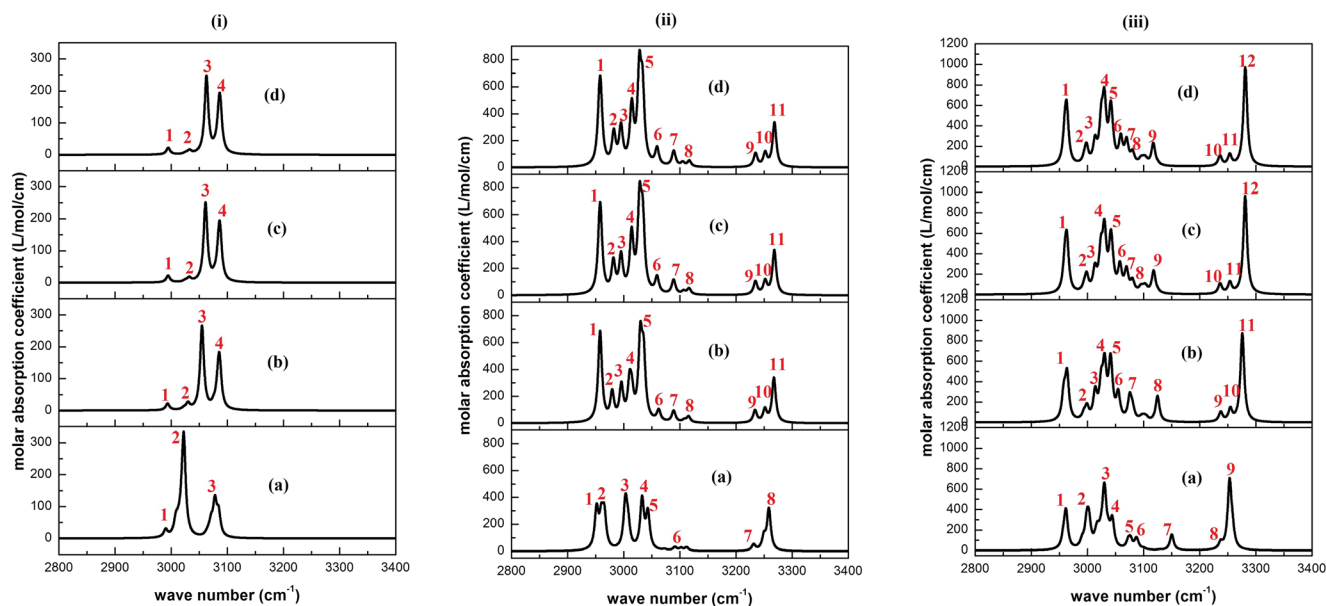


Fig. 4 Partial IR spectra (simulated) of (i) β -PVDF, (ii) [BMIM][BF₄], (iii) β -PVDF/[BMIM][BF₄] showing C–H stretching modes only (a) in gas phase, (b) solvated with THF, (iii) solvated with acetone, and (iv) solvated with DMF. [Simulation method: B3LYP-D/6–311+G(d,p)]

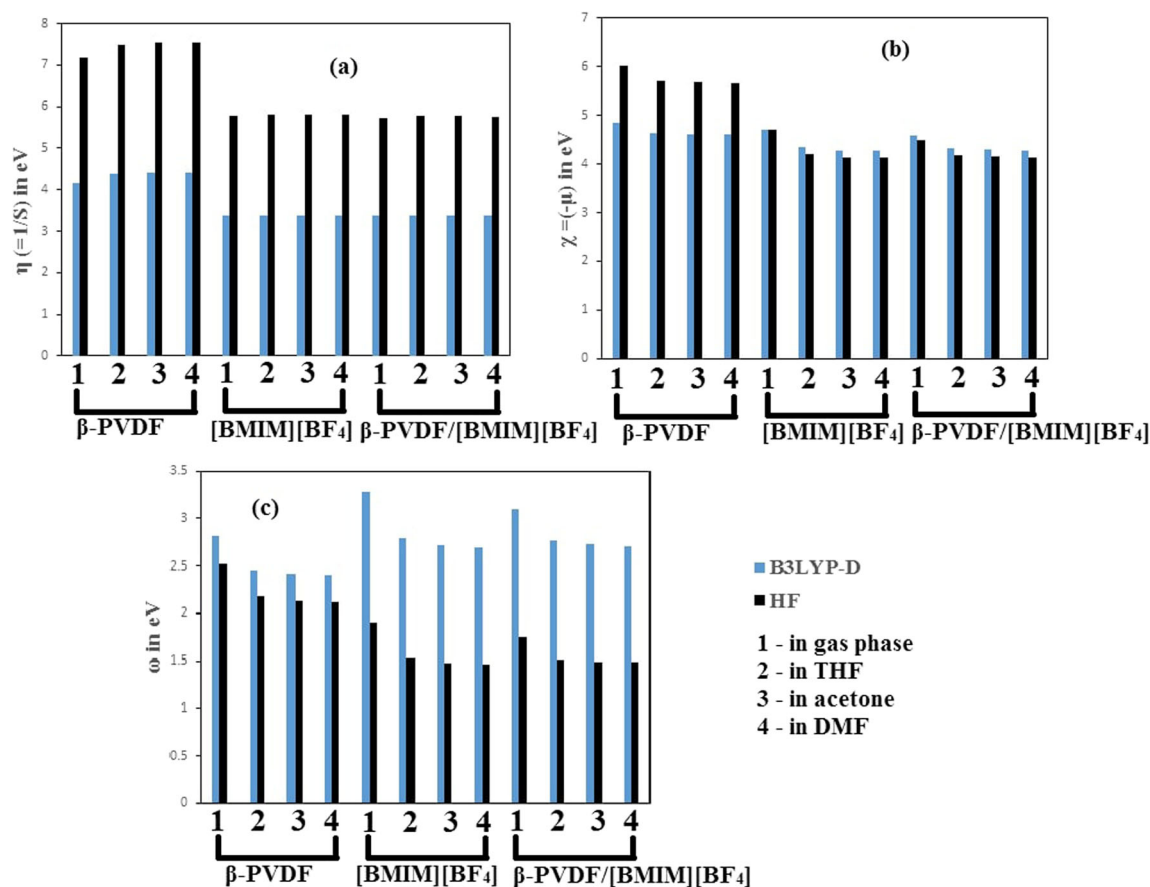


Fig. 5 Comparison of the (a) chemical hardness η (or reciprocal of chemical softness S), (b) electronegativity χ (or negative of chemical potential μ), and (c) electrophilicity index ω values as obtained from

B3LYP-D, 6-311+G(d,p), and HF, 6-311+G(d,p) methods for isolated β -PVDF, isolated [BMIM][BF₄], and β -PVDF/[BMIM][BF₄] complex systems in gas and solution phases

methods (Fig. 5). In the case of the isolated β -PVDF molecule, HOMO moves down and LUMO goes up, increasing E_{gap} value after solvation. The decrease and increase in HOMO and LUMO energies, respectively, are proportional to the solvent polarity (Table 5). In the case of [BMIM][BF₄], both HOMO and LUMO levels increase with solvent polarity, keeping the E_{gap} value almost constant. For the β -PVDF/[BMIM][BF₄] molecule, both HOMO and LUMO move up in proportion with the solvent polarity but a very small reduction in magnitude of E_{gap} occurs upon solvation. Interestingly, the HOMO-LUMO gap of isolated IL and β -PVDF/IL molecules are found to be almost equal. A larger value of E_{gap} implies higher hardness and likewise, higher chemical stability, i.e., restriction of the charge-transfer by opposing the change in electron density distribution, or reduction in polarizability. However, both the gas phase and solvation model calculations show that the isolated β -PVDF molecule possesses the highest chemical stability with respect to IL and β -PVDF/IL systems, i.e., addition of ionic liquids reduces the hardness of the β -PVDF molecule, thereby increasing the polarizability. Electronegativity and electrophilicity indices

of the all the systems are found to decrease upon solvation. Notably, chemical hardness values obtained from HF of the systems are found to be higher than B3LYP-D calculations, but electronegativity and electrophilicity indices calculated from the HF method are found to be higher in the case of B3LYP-D calculations (Fig. 5).

Weak interaction analysis

Quantitative description of the weak nonbonding interactions occurring within the β -PVDF/[BMIM][BF₄] molecular complex (within gas and solution phase) is provided with the help of five different noncovalent interaction analysis schemes, namely 1. NBO analysis, 2. Bader's QTAIM analysis, 3. Calculation of delocalization indices, 4. Hirshfeld surface analysis, and 5. NCI analysis with RDG isosurface plot. Total stabilization energy values ($E^{(2)}$), derived from inter-unit NBO analysis are given in Table 6, which suggest relatively larger $E^{(2)}$ corresponding to [BF₄]⁻/ β -PVDF interaction ($E^{(2)} = 6.68 \text{ kcal mol}^{-1}$ in the gas phase and $\sim 6.62 \text{ kcal mol}^{-1}$ within solution) than in the case of [BMIM]⁺/ β -PVDF interaction ($E^{(2)} = 5.40 \text{ kcal mol}^{-1}$ in the gas phase, $5.08 \text{ kcal mol}^{-1}$

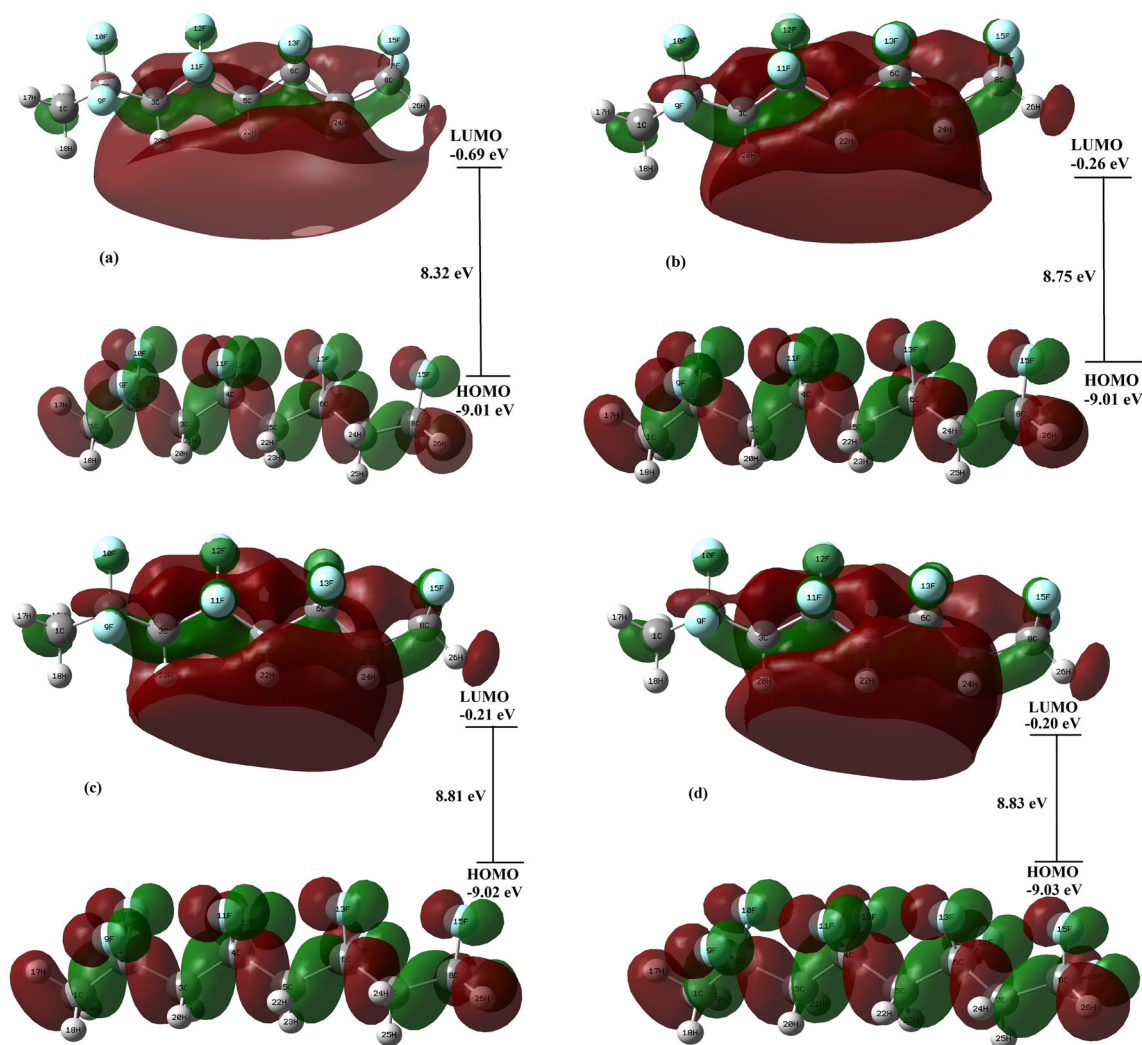


Fig. 6 HOMO-LUMO distribution in pristine β -PVDF within (a) gas phase, and solvated phase with (b) THF, (c) acetone, and (d) DMF. Simulation method: B3LYP-D/6-311+G(d,p)

in THF, 4.85 kcal mol⁻¹ in acetone, and 4.86 kcal mol⁻¹ in DMF). As $E^{(2)}$ values are directly proportional to the intensity of NBO interaction, the present NBO analysis infers better interaction of β -PVDF with IL-anion than with IL-cation. $[\text{BF}_4]^-/\beta$ -PVDF interaction is majorly dominated by electron delocalization from anion $[\text{BF}_4]^-$ to β -PVDF ($E_{[\text{BF}_4]^- \rightarrow \beta\text{PVDF}}^{(2)} = 6.47$ kcal mol⁻¹ in the gas phase, and ~ 6.35 kcal mol⁻¹ in solution phase), which is stabilized by $n \rightarrow \sigma^*$ interaction where the lone pairs of the F atoms in the anion provide the donor NBOs and the CH_2 pairs within the PVDF molecule provide the acceptor NBO. Highest $E^{(2)}$ ($= 2.41$ kcal mol⁻¹ in gas phase and ~ 2.3 kcal mol⁻¹ within solvent) is observed for interaction between lone pairs of F54 as donor and $\sigma_{\text{C5-H23}}^*$ as acceptor NBO. Notably, total $E^{(2)}$ corresponding to NBO interactions from β -PVDF fragment to anion $[\text{BF}_4]^-$ fragment is found to be much less ($E_{\beta\text{PVDF} \rightarrow [\text{BF}_4]^-}^{(2)} = 0.21$ kcal mol⁻¹ in the gas phase and

~ 0.28 kcal mol⁻¹ within solvent). On the other hand, in the case of $[\text{BMIM}]^+/\beta$ -PVDF interaction, both PVDF and IL cation contributes considerably as donor and acceptor NBOs ($E_{[\text{BMIM}]^+ \rightarrow \beta\text{PVDF}}^{(2)} = 2.46$ kcal mol⁻¹ in gas phase, 2.31 kcal mol⁻¹ in THF, 2.10 kcal mol⁻¹ in acetone, and 2.12 kcal mol⁻¹ in DMF. $E_{\beta\text{PVDF} \rightarrow [\text{BMIM}]^+}^{(2)} = 2.94$ kcal mol⁻¹ in gas phase and ~ 2.75 kcal mol⁻¹ within solvent). For $[\text{BMIM}]^+$ to β -PVDF interaction, the highest $E^{(2)}$ value (0.48 kcal mol⁻¹ in gas phase and 0.47 kcal mol⁻¹ within solvent) is associated with $\sigma_{\text{C-H}}$ donor NBO in the butyl chain attached to the imidazolium ring of the IL cation and $\sigma_{\text{C-H}}^*$ acceptor NBO in the CH_2 group of the PVDF molecule. In the case of β -PVDF to $[\text{BMIM}]^+$ interaction, the highest electron delocalization ($E^{(2)} = 0.68$ kcal mol⁻¹ in gas phase and ~ 0.65 kcal mol⁻¹ within solvent) occurs from the lone pairs of the F atoms within the CF_2 groups of PVDF molecule to $\sigma_{\text{C-H}}^*$ ($n \rightarrow \sigma^*$ interaction) and $\pi_{\text{C=C}}^*$ ($n \rightarrow \pi^*$ interaction) bonds.

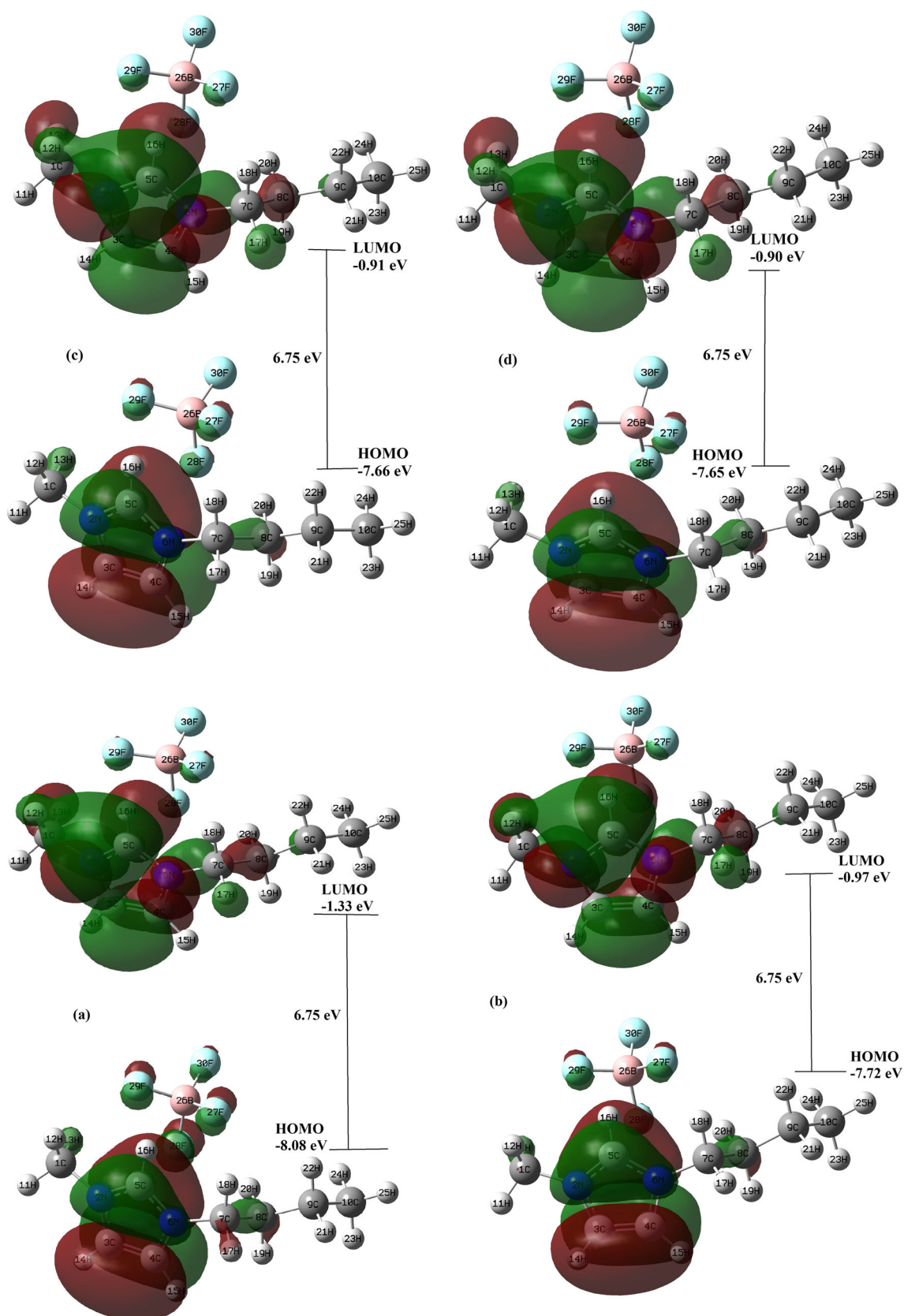


Fig. 7 HOMO-LUMO distribution in [BMIM][BF₄] molecule within (a) gas phase, and solvated phase with (b) THF, (c) acetone, and (d) DMF. Simulation method: B3LYP-D/6-311+G(d,p)

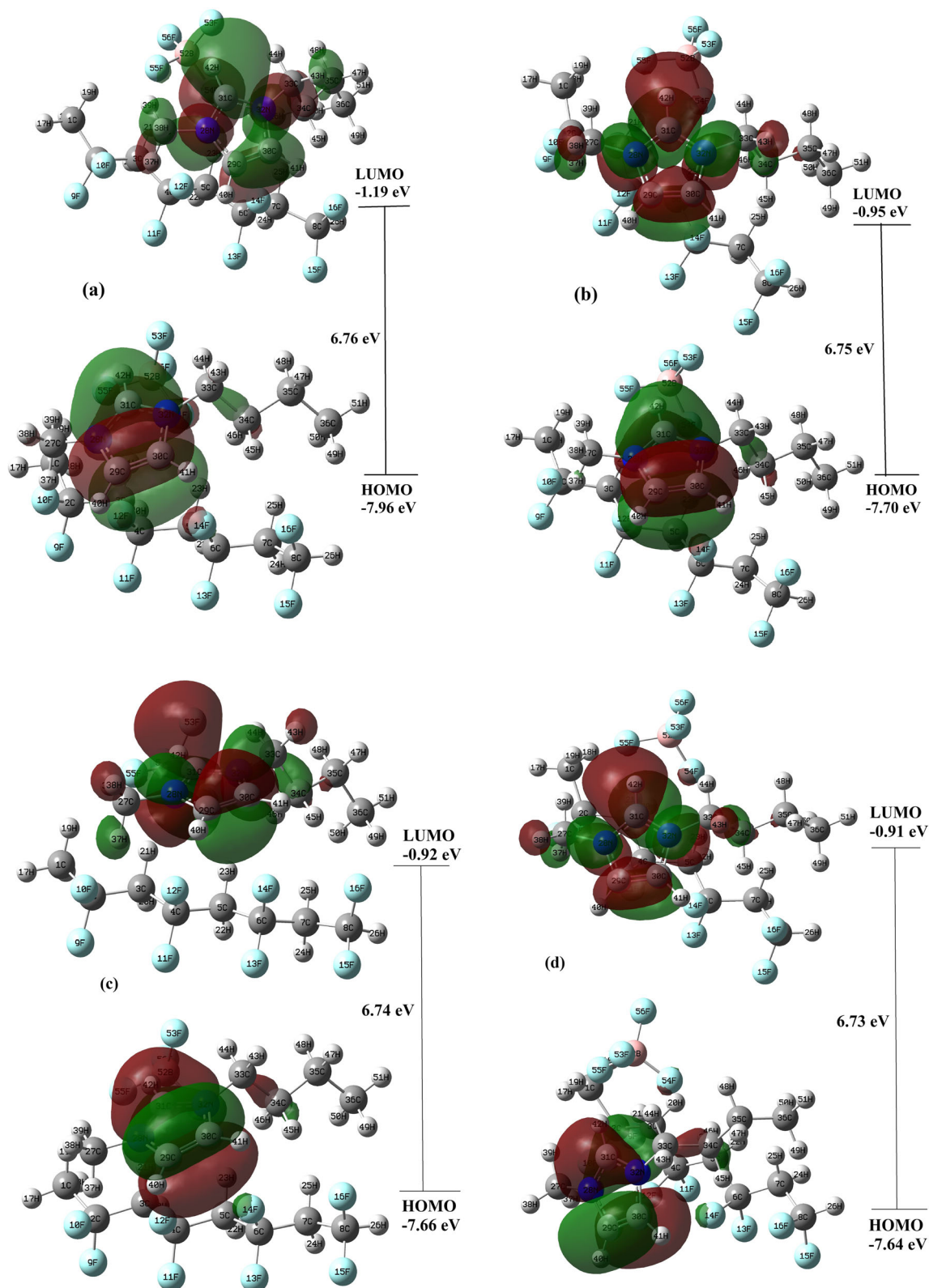


Fig. 8 HOMO-LUMO distribution in β -PVDF/[BMIM][BF₄] molecule within (a) gas phase, and solvated phase with (b) THF, (c) acetone, and (d) DMF. Simulation method: B3LYP-D/6-311+G(d,p)

However, both [BMIM]⁺/ β -PVDF and [BF₄]⁻/ β -PVDF interactions are found to decrease with the increase in solvent

polarity, which is consistent with the interaction energy values as explained in the “Energy calculations” section. Donor and

Table 5 Different chemical parameters [ionization energy (IE), electron affinity (EA), HOMO-LUMO gap (E_{gap}), electronegativity (χ), chemical potential (μ), chemical hardness (η), chemical softness (s), electrophilicity index (ω)] obtained from HOMO-LUMO energies. [simulation method: B3LYP-D, basis set: 6-311+G(d,p)]

System		IE (eV)	EA (eV)	E_{gap} (eV)	χ (eV)	μ (eV)	η	s	ω
β -PVDF	In gas phase	9.006	0.690	8.316	4.848	-4.848	4.158	0.240	2.826
	In THF	9.014	0.261	8.752	4.637	-4.637	4.376	0.229	2.457
	In acetone	9.022	0.208	8.814	4.615	-4.615	4.407	0.227	2.417
	In DMF	9.025	0.196	8.830	4.610	-4.610	4.415	0.227	2.407
[BMIM][BF ₄]	In gas phase	8.084	1.335	6.749	4.709	-4.709	3.374	0.296	3.286
	In THF	7.716	0.972	6.745	4.344	-4.344	3.372	0.297	2.790
	In acetone	7.657	0.911	6.746	4.2834	-4.2834	3.373	0.296	2.720
	In DMF	7.646	0.889	6.757	4.268	-4.268	3.379	0.296	2.695
β -PVDF/[BMIM][BF ₄]	In gas phase	7.958	1.195	6.763	4.576	-4.576	3.382	0.296	3.096
	In THF	7.705	0.950	6.755	4.327	-4.327	3.377	0.296	2.772
	In acetone	7.660	0.920	6.740	4.290	-4.290	3.370	0.297	2.730
	In DMF	7.644	0.907	6.737	4.276	-4.276	3.369	0.297	2.713

acceptor NBOs associated with the highest $E^{(2)}$ values are shown in Fig. 9 for gas phase calculations. [Refer to supplementary Fig. S4–S6 for NBO plots in the solution phase]. NBO charges of the carbon and hydrogen atoms (proton donors) forming the antibonding orbitals are provided in Table 7. A considerable increase in charge population for all the C and

H atoms forming $\sigma_{\text{C-H}}^*$ corresponding to $n \rightarrow \sigma^*$ stabilization is observed after complex formation, which is a property of proper hydrogen bond (red shifting) donors [64]. On the contrary, C atoms (C29 and C30) forming $\pi_{\text{C=C}}^*$ orbital, in the case of $n \rightarrow \pi^*$ interaction, are found to decrease upon complexation, which is consistent with the blue shift of C=C stretching

Table 6 Stabilization energy ($E^{(2)}$) corresponding to relatively higher inter-unit NBO interaction regions and total $E^{(2)}$ for inter-unit NBO interaction within the β -PVDF/[BMIM][BF₄] complex. [Refer to Figs. 1 and 2 for the atom levels]

Donor NBO	Within fragment	Type	Acceptor NBO	Within fragment	Type	$E^{(2)}$ (kcal mol ⁻¹)			
						Gas phase	In THF	In acetone	In DMF
(a) [BMIM] ⁺ / β -PVDF interaction									
LP F10	β -PVDF	n	BD* C27-H37	[BMIM] ⁺	σ^*	0.33	0.32	0.31	0.31
LP F12	β -PVDF	n	BD* C29-C30	β -PVDF	π^*	0.22	0.21	0.21	0.21
LP F14	β -PVDF	n	BD* C29-C30	β -PVDF	π^*	0.42	0.42	0.42	0.42
LP F14	β -PVDF	n	BD* C34-H45	β -PVDF	σ^*	—	—	0.15	0.15
LP F16	β -PVDF	n	BD* C34-H45	β -PVDF	σ^*	0.68	0.66	0.66	0.65
LP F16	β -PVDF	n	BD* C36-H49	β -PVDF	σ^*	0.27	0.27	0.26	0.26
BD C36-H50	[BMIM] ⁺	σ	BD* C7-H25	β -PVDF	σ^*	0.48	0.47	0.47	0.47
$E_{\beta\text{PVDF} \rightarrow [\text{BMIM}]^+}^{(2)}$						2.94	2.77	2.75	2.74
$E_{[\text{BMIM}]^+ \rightarrow \beta\text{PVDF}}^{(2)}$						2.46	2.31	2.10	2.12
Total $E^{(2)}$ for [BMIM] ⁺ / β -PVDF interaction						5.40	5.08	4.85	4.86
(b) [BF ₄] ⁻ / β -PVDF interaction									
LP F54	[BF ₄] ⁻	n	BD* C5-H23	β -PVDF	σ^*	2.41	2.33	2.32	2.31
LP F54	[BF ₄] ⁻	n	BD* C3-H21	β -PVDF	σ^*	0.92	0.90	0.90	0.90
LP F55	[BF ₄] ⁻	n	BD* C1-H19	β -PVDF	σ^*	0.79	0.78	0.79	0.78
LP F55	[BF ₄] ⁻	n	BD* C3-H21	β -PVDF	σ^*	1.14	1.12	1.12	1.12
$E_{\beta\text{PVDF} \rightarrow [\text{BF}_4]^-}^{(2)}$						0.21	0.27	0.28	0.28
$E_{[\text{BF}_4]^- \rightarrow \beta\text{PVDF}}^{(2)}$						6.47	6.35	6.35	6.34
Total $E^{(2)}$ for [BF ₄] ⁻ / β -PVDF interaction						6.68	6.62	6.63	6.62

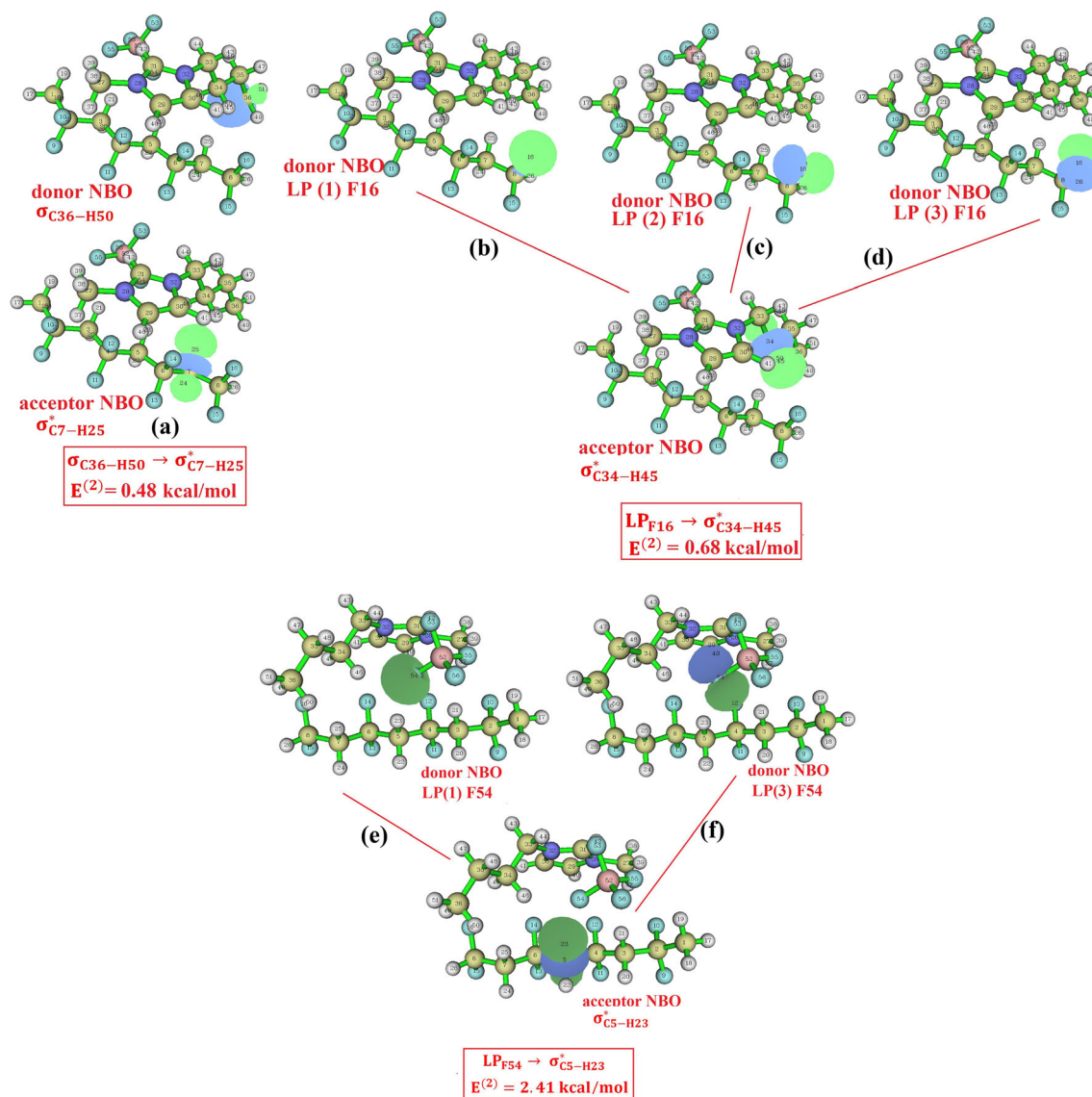


Fig. 9 NBOs corresponding to highest $E^{(2)}$ values for (a) $[\text{BMIM}]^+ \rightarrow \beta\text{-PVDF}$ interaction; (b), (c), (d) $\beta\text{-PVDF} \rightarrow [\text{BMIM}]^+$ interaction; (e), (f) $[\text{BF}_4]^- \rightarrow \beta\text{-PVDF}$ interaction within $\beta\text{-PVDF}/[\text{BMIM}][\text{BF}_4]$ in gas phase

vibration modes [64, 65]. [NBOs corresponding to $n \rightarrow \pi^*$ interaction in gas phase are shown in Fig. 10 and for solution phases refer to supplementary Fig. S7].

Inter-unit weak interaction is further investigated by Bader's QTAIM. The molecular graphs of the PVDF/IL systems within gas phase and solution phase showing the positions of bond critical points (BCP) are provided in Fig. 11. The real space functions obtained at the BCPs at the hydrogen bond interaction sites (as given in Figs. 1 and 2) are presented in Table 8. Two conditions of noncovalent interaction, i.e., $(G/|V|) > 1$ and $\nabla^2\rho > 0$ are satisfied for all the aforementioned cases as shown in Table 8. Although the concept of molecular graph (bond paths and BCPs) has been considered as a very useful method to quantify the intensity of inter-unit

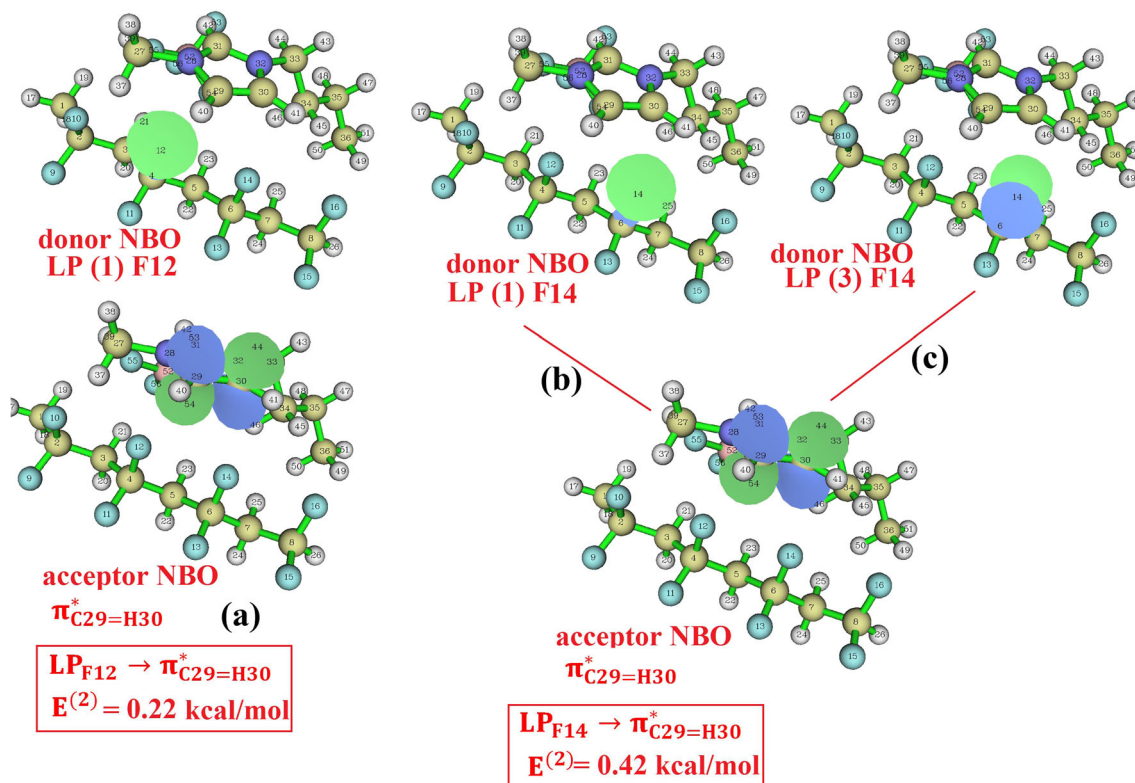
interactions in quite a number of studies [54, 66–69], some recent cases [70, 71] have questioned the reliability of this method. This is because the existence of bond paths is directly related to a large value of exchange correlation energy, which is short range in nature. Therefore, long range interactions cannot be properly explained by bond paths. BCP analysis is applicable only for a certain group of systems with $\text{D-H}\cdots\text{A}$, where both D and A are the same within the group. Notably, as the present systems under study contain only $\text{C-H}\cdots\text{F}$ type hydrogen bonds, the electron density values located within $\text{H}\cdots\text{F}$ bonds can be correlated to the hydrogen bond strength. Besides, in the present cases, existence of bond paths is in good correspondence with the presence in hydrogen bonds. For example, in the gas phase, the bond length of $14\text{F}\cdots 45\text{H}$ is not within the $\text{H}\cdots\text{F}$ hydrogen bond distance and there is no

Table 7 NBO charges of the atoms forming antibonding orbitals associated with comparatively higher stabilization energy in NBO interaction. [Refer to Figs. 1 and 2 for the atom levels]

Antibonding orbitals	Atoms	NBO charges							
		In gas phase		In THF		In acetone		In DMF	
		Isolated state	Complex state	Isolated state	Complex state	Isolated state	Complex state	Isolated state	Complex state
σ_{C1-H19}^*	C1	-0.626	-0.634	-0.631	-0.637	-0.632	-0.635	-0.632	-0.635
	H19	0.215	0.244	0.225	0.241	0.227	0.237	0.228	0.237
σ_{C3-H21}^*	C3	-0.491	-0.515	-0.502	-0.522	-0.505	-0.522	-0.505	-0.522
	H21	0.228	0.271	0.245	0.274	0.249	0.272	0.250	0.272
σ_{C5-H23}^*	C5	-0.489	-0.510	-0.500	-0.511	-0.502	-0.513	-0.503	-0.513
	H23	0.227	0.268	0.246	0.262	0.250	0.263	0.251	0.263
$\sigma_{C27-H37}^*$	C27	-0.352	-0.362	-0.351	-0.355	-0.351	-0.356	-0.350	-0.356
	H37	0.200	0.237	0.217	0.233	0.220	0.233	0.220	0.232
$\sigma_{C34-H45}^*$	C34	-0.406	-0.411	-0.403	-0.409	-0.403	-0.411	-0.403	-0.411
	H45	0.184	0.206	0.195	0.212	0.198	0.213	0.198	0.214
$\sigma_{C36-H49}^*$	C36	-0.572	-0.573	-0.573	-0.577	-0.574	-0.578	-0.574	-0.578
	H49	0.190	0.196	0.194	0.196	0.195	0.197	0.196	0.197
$\pi_{C29-C30}^*$	C29	-0.016	-0.009	-0.015	-0.012	-0.015	-0.011	-0.015	-0.011
	C30	-0.018	-0.013	-0.020	-0.009	-0.020	-0.008	-0.020	-0.008

bond path in the molecular graph. However, in the solution phase, bond paths are observed in this atom pair and the bond lengths are also within $H \cdots F$ hydrogen bond distance.

According to the electron density values mentioned in Table 8, relatively stronger hydrogen bonds are formed in the case of $[BF_4]^-/\beta$ -PVDF than $[BMIM]^+/\beta$ -PVDF.

**Fig. 10** NBOs corresponding to $n \rightarrow \pi^*$ interaction occurring between β -PVDF and $[BMIM]^+$ in gas phase

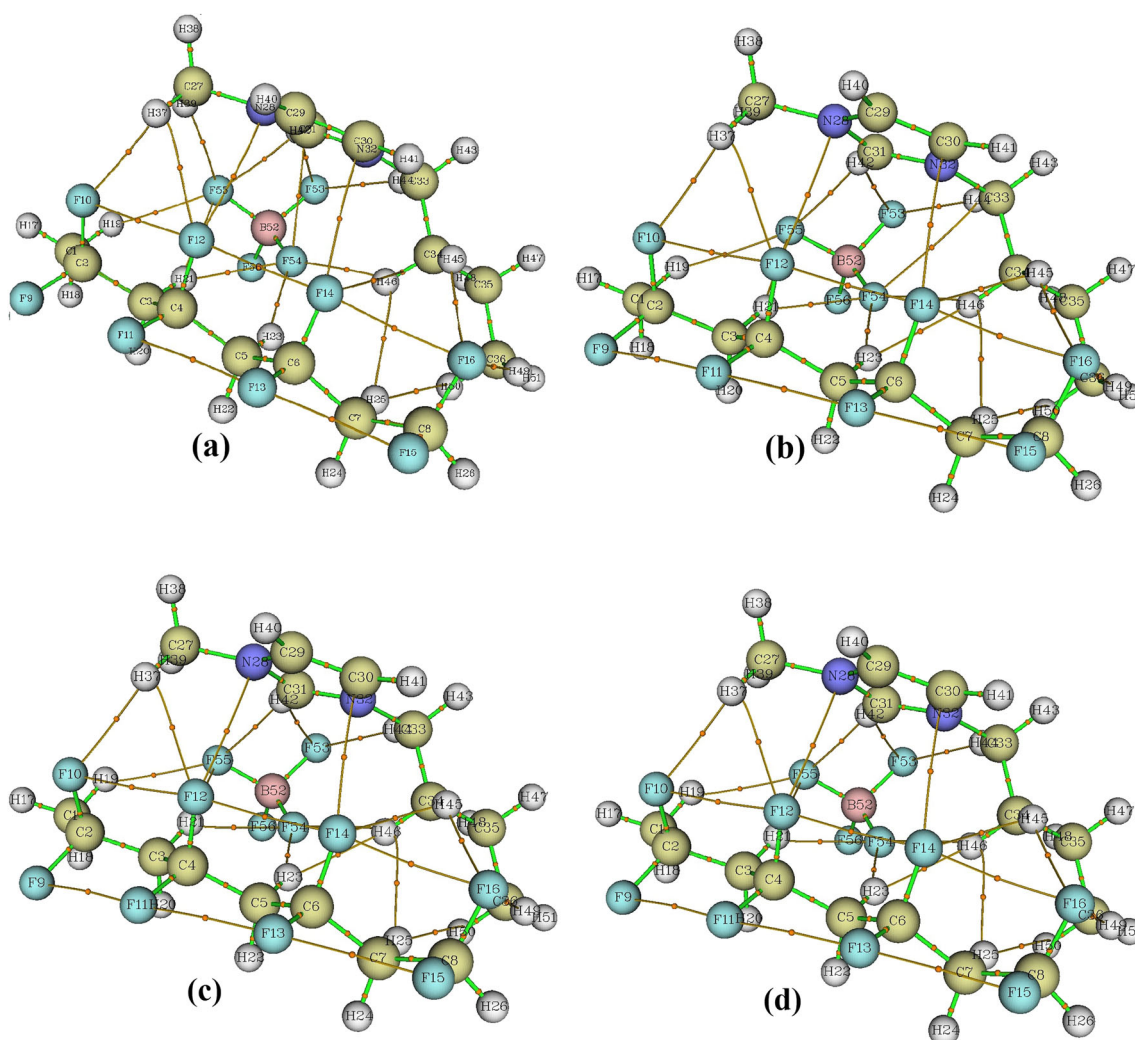


Fig. 11 Molecular graphs of β -PVDF/[BMIM][BF₄] molecules based on QTAIM analysis (a) in gas phase, (b) solvated with THF, (c) solvated with acetone, and (d) solvated with DMF. The orange dots indicate the bond critical points (BCP) and the yellow lines refer to the bond paths

Electron density values are found to decrease after solvation (except for C1–H19...F55 bond, which shows negligible increase in electron density value within THF solvent [refer Table 8(d)]), which indicates reduced inert-unit interaction within molecular complex upon solvation and this fact is exactly in good agreement with the NBO analysis discussed before.

However, to avoid the confusion regarding the QTAIM method as discussed above, and to provide a more generalized description, interacting quantum atoms (IQA) approach [25, 72] has been introduced where the global quantities (doubly integrated, or domain-averaged) are calculated instead of considering the local values of the real space functions at the BCPs. As given in Eq. 22, the delocalization index (DI) is a parameter obtained from domain-averaged exchange correlation energy density, which can be used as a more reliable approach to study the nonbonding interactions. Delocalization indices are conventionally calculated in AIM space but in the current study the calculations are done in the

fuzzy atomic space to reduce the computational cost [47, 73]. Magnitudes of DI values are directly correlated to strength of a bond. DI values of the hydrogen-bonded atom pairs within the systems are calculated and given in Table 9.

To provide further insight into weak interactions, Hirshfeld surface analysis is carried out. Electron density values (ρ) mapped onto the Hirshfeld surface are plotted between [BMIM][BF₄] and β -PVDF fragments of β -PVDF/[BMIM][BF₄] complex in the gas phase and shown in Fig. 12 [refer to supplementary Figs. S8–S10 for the Hirshfeld surfaces of systems in the solution phases]. Red zones on the Hirshfeld surface refer to the high ρ regions that appear between the [BF₄][−] anion and β -PVDF fragments [refer to Fig. 12] and indicate relatively higher electron density (i.e., better inter-fragment interactions) at those regions.

To obtain the Hirshfeld fingerprint plot, the β -PVDF unit of the β -PVDF/IL molecule (in the gas phase) is defined as the inside fragment and promolecular electron density is considered as the mapped function. Three spikes are observed in the

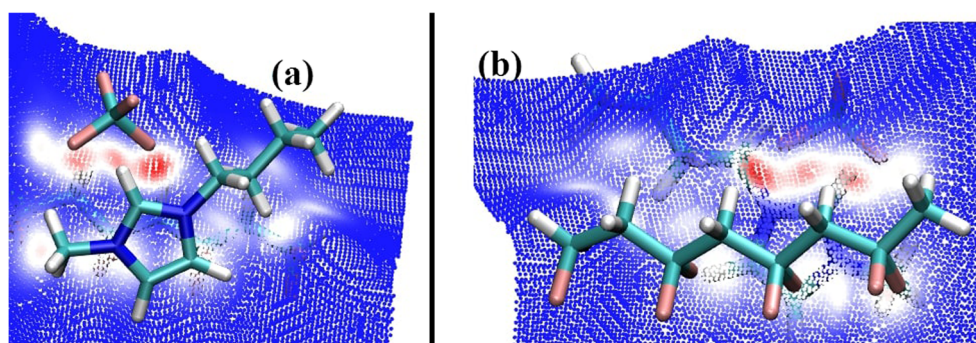
Table 8 Real space functions calculated at the BCPs corresponding to comparatively higher interaction [Refer to Figs. 1 and 2 for the atom levels]

X–H···Y	ρ	$\nabla^2\rho$	G	V	H	$G/ V $
(a) [BMIM] ⁺ /β-PVDF interaction in gas phase						
C27–H37···F10	0.00917	0.03702	0.00790	−0.00654	0.00136	1.208
C29=C30···F14	0.00878	0.03582	0.00763	−0.00630	0.00133	1.211
C34–H45···F16	0.00849	0.03094	0.00678	−0.00583	0.00095	1.163
C36–H49···F16	0.00645	0.02307	0.00501	−0.00426	0.00076	1.176
(b) [BF ₄] [−] /β-PVDF interaction in gas phase						
C5–H23···F54	0.01520	0.05837	0.01282	−0.01105	0.00177	1.160
C3–H21···F54	0.01138	0.04230	0.00922	−0.00787	0.00135	1.171
C3–H21···F55	0.01189	0.04377	0.00957	−0.00820	0.00137	1.167
C1–H19···F55	0.00813	0.02948	0.00637	−0.00536	0.00100	1.188
(c) [BMIM] ⁺ /β-PVDF interaction in THF						
C27–H37···F10	0.00842	0.03325	0.00712	−0.00592	0.00120	1.202
C29=C30···F14	0.00736	0.02945	0.00622	−0.00507	0.00115	1.227
C34–H45···F14	0.00697	0.02843	0.00597	−0.00485	0.00113	1.231
C34–H45···F16	0.00840	0.03157	0.00662	−0.00570	0.00092	1.161
C36–H49···F16	0.00580	0.02090	0.00450	−0.00378	0.00072	1.190
(d) [BF ₄] [−] /β-PVDF interaction in THF						
C5–H23···F54	0.01066	0.04065	0.00873	−0.00737	0.00360	1.185
C3–H21···F54	0.01130	0.04148	0.00910	−0.00783	0.00127	1.162
C3–H21···F55	0.01165	0.04218	0.00928	−0.00801	0.00127	1.159
C1–H19···F55	0.00837	0.03044	0.00659	−0.00558	0.00102	1.181
(e) [BMIM] ⁺ /β-PVDF interaction in acetone						
C27–H37···F10	0.00859	0.03301	0.00710	−0.00595	0.00115	1.193
C29=C30···F14	0.00730	0.02884	0.00609	−0.00497	0.00112	1.225
C34–H45···F14	0.00720	0.02823	0.00601	−0.00497	0.00104	1.209
C34–H45···F16	0.00829	0.02968	0.00654	−0.00560	0.00091	1.168
C36–H49···F16	0.00624	0.02219	0.00482	−0.00410	0.00072	1.176
(f) [BF ₄] [−] /β-PVDF interaction in acetone						
C5–H23···F54	0.01097	0.04179	0.00904	−0.00762	0.00141	1.186
C3–H21···F54	0.01027	0.03831	0.00836	−0.00714	0.00122	1.171
C3–H21···F55	0.01178	0.04235	0.00934	−0.00801	0.00098	1.166
C1–H19···F55	0.00774	0.02866	0.00618	−0.00520	0.00124	1.188
(g) [BMIM] ⁺ /β-PVDF interaction in DMF						
C27–H37···F10	0.00852	0.03268	0.00703	−0.00589	0.00114	1.194
C29=C30···F14	0.00718	0.02837	0.00598	−0.00488	0.00111	1.225
C34–H45···F14	0.00725	0.02839	0.00606	−0.00501	0.00104	1.210
C34–H45···F16	0.00825	0.02956	0.00649	−0.00558	0.00091	1.163
C36–H49···F16	0.00616	0.02194	0.00476	−0.00404	0.00072	1.178
(h) [BF ₄] [−] /β-PVDF interaction in DMF						
C5–H23···F54	0.01084	0.04127	0.00892	−0.00752	0.00140	1.186
C3–H21···F54	0.01020	0.03807	0.00831	−0.00708	0.00122	1.315
C3–H21···F55	0.01171	0.04210	0.00928	−0.00804	0.00124	1.154
C1–H19···F55	0.00767	0.02846	0.00613	−0.00515	0.00098	1.190

overall hirshfeld fingerprint plot, as shown in Fig. 13a, which infers that β-PVDF acts as both a hydrogen bond donor and acceptor. To provide distinct descriptions of each of the spikes, the total fingerprint plot is decomposed for local contact points

between particular atoms of three fragments (β-PVDF, [BMIM]⁺, [BF₄][−]) and shown in Fig. 13b-d. Figure 13b is the fingerprint plot of the contact surface between the F atoms of β-PVDF and H atoms of [BMIM]⁺ corresponding to spike

Fig. 12 Hirshfeld surface mapped onto the electron density for β -PVDF/[BMIM][BF₄] in gas phase. [(a) and (b) are provided for convenient visualization of both fragments]



1, where $d_i > d_c$, i.e., β -PVDF behaves like a hydrogen bond acceptor. Spike 2 is observed at the $d_i \sim d_c$ region, which is obtained from the fingerprint plot between the H atoms of β -PVDF and H atoms of [BMIM]⁺, as separately shown in Fig. 13c. Figure 13d corresponds to spike 3 ($d_i < d_c$), which shows the local contact regions between H atoms of β -PVDF and F atoms of [BF₄]⁻, suggesting the hydrogen bond donor property of β -PVDF. Thus, three spikes in the overall Hirshfeld fingerprint plot demonstrate F \cdots H, H \cdots H, and H \cdots F inter-unit interactions, respectively. Hirshfeld fingerprint plots of the β -PVDF/IL system in the solution phases are provided in supplementary Figs. S11–S13. The percentage of contributions of each type of interactions to the total Hirshfeld surface are mentioned in Fig. 13. It is observed that the highest contribution (49.51% in gas phase, 49.92% in THF, 48.77% in acetone, and 48.61% in DMF) is associated with the F \cdots H interaction occurring between the F atoms of the β -PVDF and H atoms of [BMIM]⁺, whereas the H \cdots F interaction between the H atom of β -PVDF and F atoms of [BF₄]⁻ units possesses the lowest contribution (20.90% in gas phase, 19.82% in THF, 18.35% in acetone, and 18.25% in DMF) to the total Hirshfeld surface. However, as evident from

Table 9 Delocalization indices of the H \cdots F atom pairs of the inter-unit H \cdots F bonds within β -PVDF/[BMIM][BF₄] systems in gas and solution phases [Refer to Figs. 1 and 2 for the atom levels]

Hydrogen bonds	Delocalization index			
	In gas phase	In THF	In acetone	In DMF
(a) [BMIM] ⁺ / β -PVDF hydrogen bonds				
37H \cdots 10F	0.02896	0.02851	0.02933	0.02919
37H \cdots 12F	0.01990	0.02145	0.02149	0.02161
45H \cdots 14F	0.01253	0.01792	0.02002	0.02024
45H \cdots 16F	0.03130	0.02997	0.02902	0.02891
49H \cdots 16F	0.03377	0.03095	0.03209	0.03181
(b) [BF ₄] ⁻ / β -PVDF hydrogen bonds				
19H \cdots 55F	0.03408	0.03675	0.03511	0.03488
21H \cdots 54F	0.02616	0.02840	0.02475	0.02458
21H \cdots 55F	0.02764	0.02970	0.03131	0.03118
23H \cdots 54F	0.04749	0.03698	0.03761	0.03724

Fig. 12, anion [BF₄]⁻/ β -PVDF interaction regions exhibit comparatively higher electron density (i.e., relatively stronger interaction) despite the lowest contribution to the total Hirshfeld surface.

Reduced density gradient plot and noncovalent interaction zones within the PVDF/IL complex in gas phase is provided in Fig. 14. [Refer to supplementary Fig. S14–S16 for NCI plots of the solvated molecules]. The majority of the prominent peaks appearing at the vicinity of zero electron density in the RDG plot as given in Fig. 14a suggest weak (van der Waals) inter-unit interaction occurring throughout the β -PVDF/IL complex. Peaks at the negative ρ side at lower density values ($|\rho| < 0.01$) indicate weak [BMIM]⁺/PVDF hydrogen bond interactions, and $|\rho| > 0.01$ region results from comparatively stronger [BF₄]⁻/PVDF hydrogen bond interactions. Some peaks appear at the positive side of the ρ -axis, which infer destabilizing (repulsive) interaction occurring at the center of the imidazolium ring of the [BMIM]⁺ cation and in between the highly electronegative fluorine atom pairs within the [BF₄]⁻ anions within the PVDF/IL complex. The NCI isosurface plot, as demonstrated in Fig. 14b, shows the inter-unit interaction regions as green isosurface (corresponding to weak van der Waals interaction) throughout the whole β -PVDF/[BMIM][BF₄] system. For clear understanding, the NCI isosurfaces corresponding to [BF₄]⁻/ β -PVDF and IL [BMIM]⁺/ β -PVDF interaction are separately provided in Fig. 13c and d, respectively.

Nature of the hydrogen bonds

All the nonbonding interaction studies mentioned above, suggest the presence of weak inter-unit hydrogen bonds within the β -PVDF/[BMIM][BF₄] system, both in gas and solution phases. Apparently, these C–H \cdots F bonds indicate proper donor-acceptor type behavior, as evident from the NBO charges as described in the “NBO analysis” section. However, as discussed in the vibrational frequency analysis, most of the C–H stretching modes show blue shift after solvation, which is considered as the nature of improper C–H hydrogen bond donors. In conventional hydrogen bonds, the D–H (D = donor) bond length of an isolated molecule

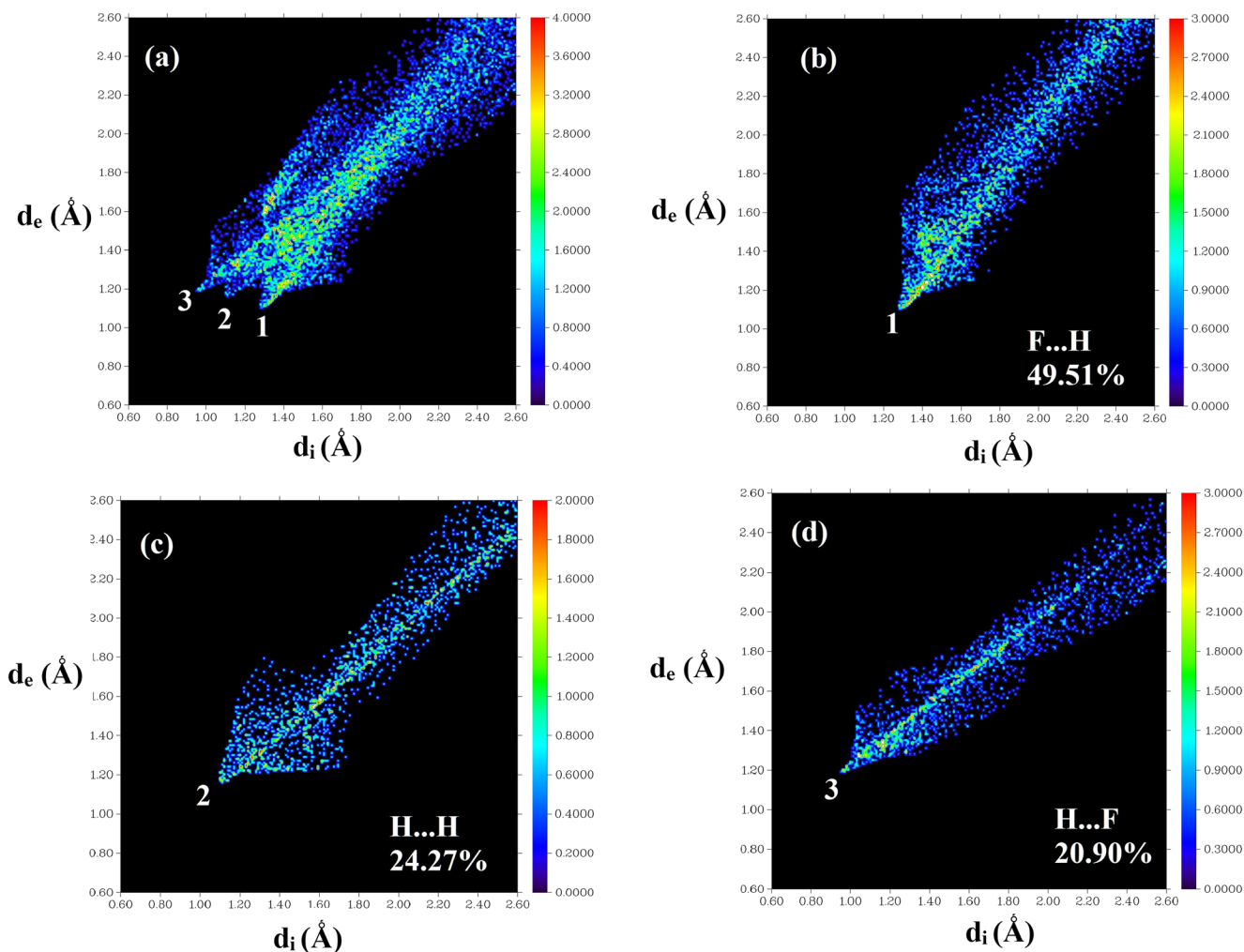


Fig. 13 Hirshfeld fingerprint plots of β -PVDF/[BMIM][BF₄] in gas phase corresponding to the contact surfaces between (a) all atoms of β -PVDF fragment and all atoms of [BMIM][BF₄], (b) F atoms of β -PVDF

fragment and H atoms of [BMIM]⁺ fragment, (c) H atoms of β -PVDF fragment and H atoms of [BMIM]⁺ fragment, (d) H atoms of β -PVDF fragment and F atoms of [BF₄]⁻ fragment

increases after complex formation. As a result, the bond becomes weaker and the electron density within the D–H atom pair reduces. However, in the case of improper C–H proton donors, the scenario is just the opposite [74–77]. Table 10 suggests that the C–H bonds within isolated β -PVDF or [BMIM][BF₄] systems become shorter after forming the β -PVDF/[BMIM][BF₄] complex, increasing the electron density at the BCP at the C–H bonds. This improper nature of C–H...F hydrogen bonds causes blue shift in the C–H stretching frequencies upon solvation, as described in the “IR spectra analysis” section.

Thermochemistry

All the thermochemical calculations for the systems under study are carried out using the frequency scaling factor of 0.9877, which is suitable for 6–311+G(d,p) [57]. Temperature dependence of thermal correction factors corresponding to total energy (E_{corr}), enthalpy (H_{corr}), and Gibbs

free energy (G_{corr}) of pure and [BMIM][BF₄] added β -PVDF in the gas phase are calculated using the freqcheck utility of the Gaussian09 program. It is observed that E_{corr} and H_{corr} values are very close to each other at all temperatures. However, these correction factors are found to show increased rate of temperature dependence for β -PVDF/[BMIM][BF₄] than for the pristine β -PVDF molecule. However, for all the systems under study, Gibbs free energy reduces with increasing temperature, which suggests higher stability of the systems at higher temperature. On the basis of the same level of theory as the previous calculations, temperature dependence of standard statistical thermodynamic functions, e.g., specific heat at constant pressure (C_p^0), entropy (S^0), and enthalpy gradient [$ddH=H^0(T)-H^0(0)$] are obtained within the temperature range 100–1000 K and 1 atm pressure. Temperature dependence of thermal correction factors and the standard thermodynamic parameters in the gas phase are shown in Fig. 15. All these standard parameters are found to increase with the increase in temperature because of the increase in molecular

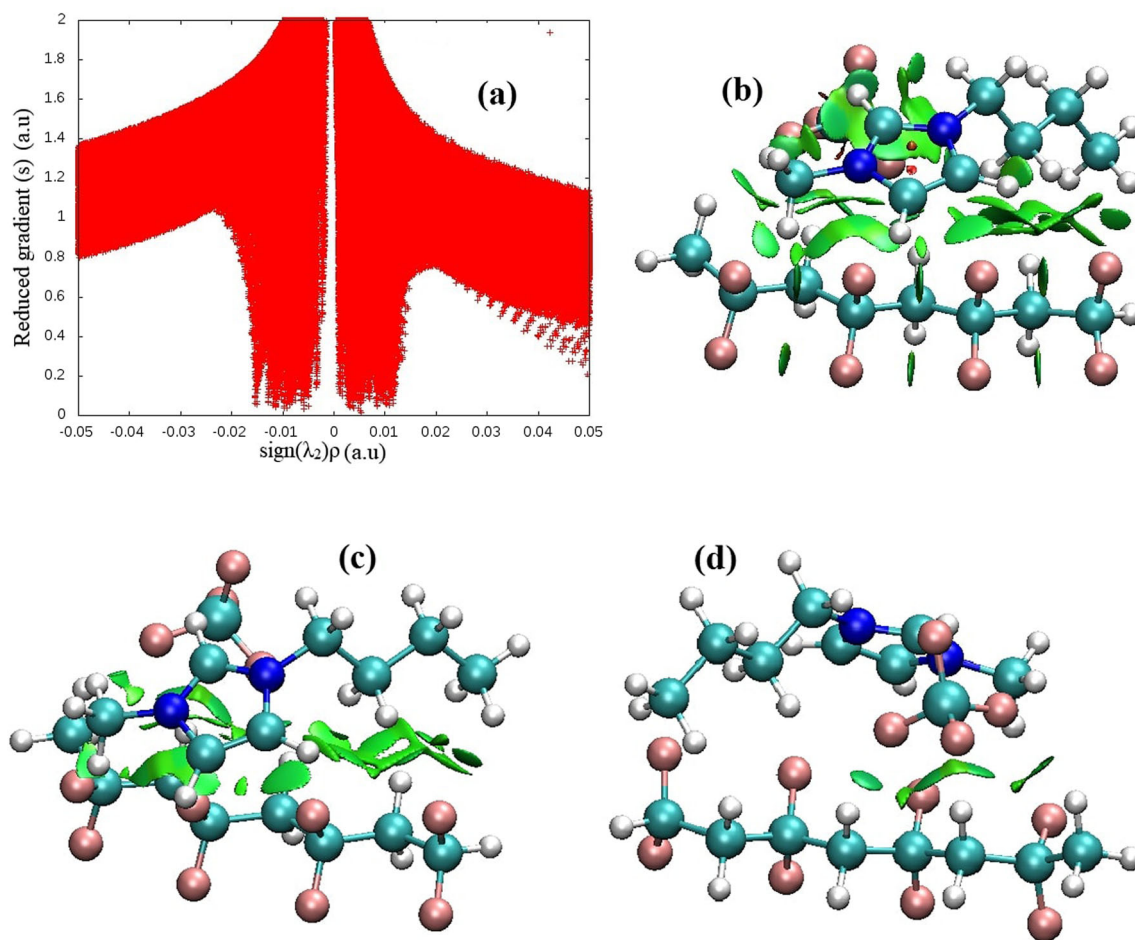


Fig. 14 NCI analysis of [BMIM][BF₄] in gas phase. **a** Reduced density gradient (*s*) vs $\text{sign}(\lambda_2)\rho$ plot for the SCF density, **b** isosurface plot showing the overall interaction (interaction among [BF₄]⁻, [BMIM]⁺,

and PVDF), **c** isosurface plot selectively showing [BMIM]⁺/β-PVDF interaction, **d** isosurface plot selectively showing [BF₄]⁻/β-PVDF interaction

vibrational intensities with the increase in temperature. Correlations of these thermodynamic parameters with temperature along with the fitting factor (R^2) are mentioned within the diagram. These equations may be helpful for further

thermodynamic study of the systems under study. [Thermochemical data of the systems in the solution phases are provided in supplementary Table S7 and supplementary Fig. S15–S17].

Table 10 Bond length and electron density at BCP within C–H atom pairs forming inter-unit C–H···F hydrogen bonds

Hydrogen bond	ρ [and bond length (Å)] in gas phase		ρ [and bond length (Å)] in THF		ρ [and bond length (Å)] in acetone		ρ [and bond length (Å)] in DMF	
	In isolated [BMIM][BF ₄]	In β-PVDF/[BMIM][BF ₄]	In isolated [BMIM][BF ₄]	In β-PVDF/[BMIM][BF ₄]	In isolated [BMIM][BF ₄]	In β-PVDF/[BMIM][BF ₄]	In isolated [BMIM][BF ₄]	In β-PVDF/[BMIM][BF ₄]
(a) For [BMIM] ⁺ /PVDF interaction [Refer to Figs. 1 and 2 for the atom levels]								
C27–H37	0.281 [1.090]	0.285 [1.088]	0.282 [1.089]	0.284 [1.088]	0.283 [1.089]	0.285 [1.088]	0.283 [1.089]	0.285 [1.088]
C34–H45	0.272 [1.097]	0.278 [1.093]	0.274 [1.096]	0.278 [1.093]	0.274 [1.096]	0.278 [1.092]	0.274 [1.095]	0.278 [1.092]
C36–H49	0.272 [1.096]	0.273 [1.094]	0.272 [1.095]	0.273 [1.095]	0.272 [1.095]	0.273 [1.094]	0.272 [1.095]	0.273 [1.094]
(b) [BF ₄] ⁻ /PVDF interaction [Refer to Figs. 1 and 2 for the atom levels]								
C1–H19	0.274 [1.092]	0.277 [1.091]	0.275 [1.092]	0.277 [1.091]	0.275 [1.092]	0.277 [1.091]	0.275 [1.091]	0.277 [1.091]
C3–H21	0.277 [1.093]	0.284 [1.087]	0.278 [1.092]	0.283 [1.088]	0.278 [1.092]	0.283 [1.089]	0.278 [1.092]	0.282 [1.089]
C5–H23	0.277 [1.093]	0.281 [1.090]	0.278 [1.092]	0.280 [1.091]	0.279 [1.092]	0.281 [1.090]	0.279 [1.092]	0.281 [1.090]

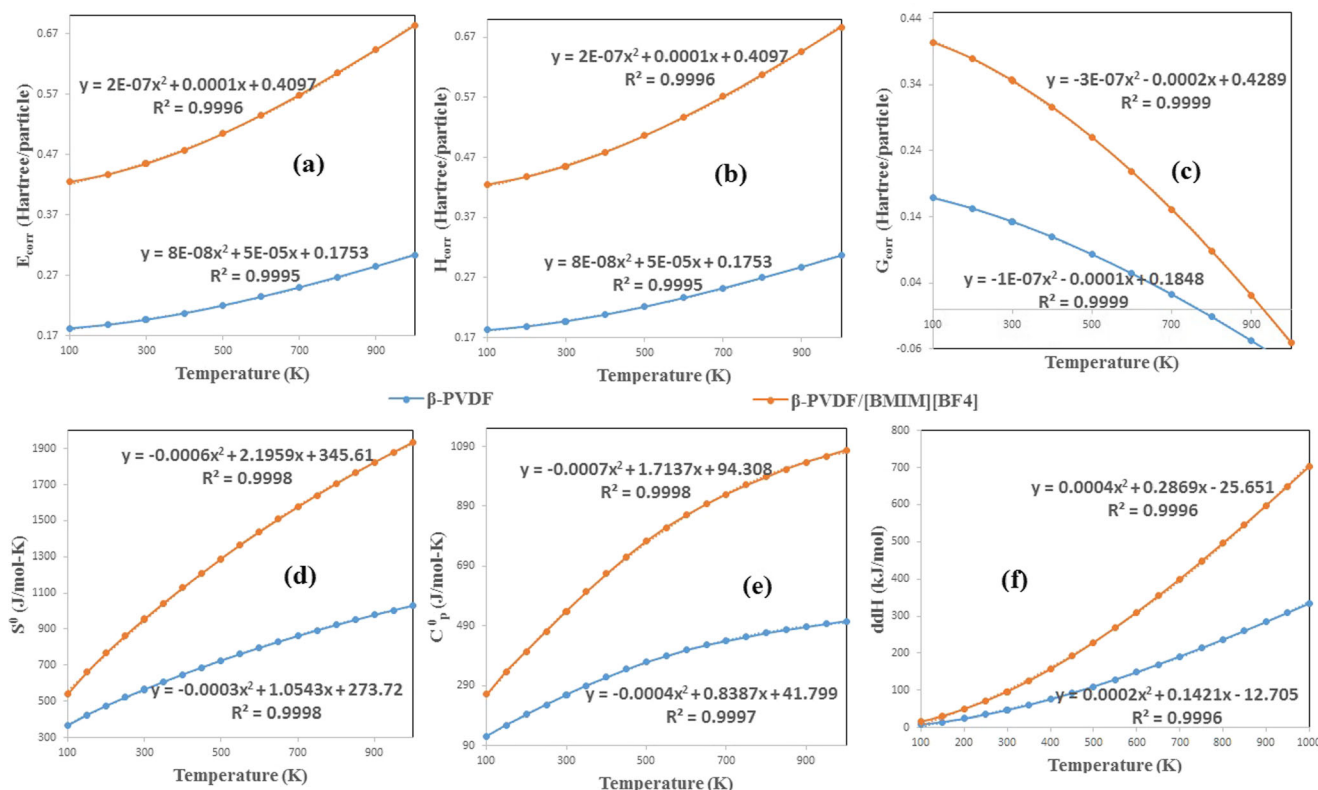


Fig. 15 Thermal correction factor of (a) total energy, (b) enthalpy, and (c) Gibbs free energy; and temperature dependence of different standard thermodynamic parameters (d) entropy S^0 , (e) heat capacity at constant

pressure C_p^0 , and (f) enthalpy gradient ddH for β -PVDF and β -PVDF/[BMIM][BF₄] complex in gas phase. Simulation method: B3LYP-D/6-311+G(d,p)

Conclusions

A detailed analysis of molecular interactions within the β -PVDF/[BMIM][BF₄] complex is performed with the help of dispersion corrected density functional theory in gas phase and in solution phase with three solvents, namely tetrahydrofuran (THF), acetone, and *n,n*-dimethyl formamide (DMF) using the integral equation formalism polarizable continuum model (IEFPCM). Structural description and vibrational frequency analyses are provided for pristine α - and β -PVDF, ionic liquid [BMIM][BF₄], and β -PVDF/[BMIM][BF₄], which have shown good agreement with available experimental results. Dipole moment and polarizability values of all the optimized structures are found to increase considerably upon solvation because of the dipole–dipole interaction between the solvent and the solute (system under study). C–H···F type hydrogen bonds are found showing [BMIM]⁺/ β -PVDF and [BF₄][−]/ β -PVDF interactions. As evident from the calculated values of binding energy, supermolecular interaction energy and SAPT energy, ionic liquid [BMIM][BF₄] shows better interaction with β -PVDF than with α -PVDF, which is demonstrated as the reason for nucleation of β -PVDF crystals out of PVDF blend (mixture of all the structural polymorphs of PVDF, majorly α phase). SAPT analysis suggests, inter-unit attractive interaction within PVDF/IL systems is majorly

electrostatic (~70%) and dispersive (~30%). HOMO-LUMO positions within PVDF/IL systems suggest better chemical reactivity of the IL than PVDF molecule. Different chemical parameters obtained from HOMO-LUMO energies are calculated according to Koopmans' theory both in B3LYP-D and HF methods. Despite the variations in the magnitudes of the calculated parameters, the trend of change of them after solvation are found to be similar in both methods. Noncovalent interaction or inter-unit interaction within PVDF/IL complex molecules are investigated with the help of NBO analysis, Bader's QTAIM, delocalization indices, Hirshfeld surface analysis, and RDG analysis. Stabilization energy ($E^{(2)}$) values obtained from second order perturbation theory analysis (NBO analysis) are found to be higher in the case of IL-anion ([BF₄][−])/PVDF interaction than IL-cation ([BMIM]⁺)/PVDF interaction. This fact is further ensured by the QTAIM study where bond critical points corresponding to IL-anion/PVDF interaction have higher electron density than BCPs for IL-cation/PVDF interaction. The inter-fragment Hirshfeld surface is generated in between the β -PVDF part and IL part and mapped onto the electron density values. Higher electron density regions are found to appear between the [BF₄][−] anion and β -PVDF. To avoid the confusion regarding the short-range behavior of the calculated real space functions at BCPs, delocalization index values, based on the IQA approach, are also

calculated to confirm the nature of the nonbonding interactions. However, both cations and anions of ionic liquids show weak van der Waals interaction with PVDF as depicted in the RDG plot and NCI isosurface plot. The inter-unit C–H···F bonds are found to show improper hydrogen bond characteristics. Finally, thermochemical calculations are carried out for pristine and IL added β -PVDF systems. A mathematical description of temperature dependence of different standard thermodynamic parameters is provided.

References

- Lines ME, Glass AM (1977) Principles and applications of ferroelectrics and related materials. Clarendon, Oxford
- Itoh A, Takahashi Y, Furukawa T, Yajima H (2014) Solid-state calculations of poly(vinylidene fluoride) using the hybrid DFT method: spontaneous polarization of polymorphs. *Polym J* 46: 207–211
- Bohlé M, Bolton K (2014) Conformational studies of poly(vinylidene fluoride), poly(trifluoroethylene) and poly(vinylidene fluoride-co-trifluoroethylene) using density functional theory. *Phys Chem Chem Phys* 16:12929–12939
- Nabata Y (1990) Structure of crosslinked poly(vinylidene fluoride) crystallized from melt under uniaxial compression. *Jpn J Appl Phys* 29:1298–1303
- Gomes J, Nunes JS, Sencadas V, Lanceros-Mendez S (2010) Influence of the β -phase content and degree of crystallinity on the piezo- and ferroelectric properties of poly(vinylidene fluoride). *Smart Mater Struct* 19:065010 1–065010 7
- Qian X, Wu S, Furman E, Zhang Q, Su J (2015) Ferroelectric polymers as multifunctional electroactive materials: recent advances, potential, and challenges. *MRS Commun* 5(2):115–129
- Abolhasani MM, Zarejousheghani F, Cheng ZX, Naebe M (2015) A facile method to enhance ferroelectric properties in PVDF nanocomposites. *RSC Adv* 5:22471–22479
- Mofokeng TG, Luyt AS, Pavlovic VP, Pavlovic VB, Dudic D, Vlahovic B, Djokovic V (2014) Ferroelectric nanocomposites of poly(vinylidene fluoride)/polymethyl methacrylate blend and BaTiO₃ particles: fabrication of β -crystal polymorph rich matrix through mechanical activation of the filler. *J Appl Phys* 115:084109 1–9
- Mahdi RI, Gan WC, Halim NA, Velayutham TS, Majid WHA (2015) Ferroelectric and pyroelectric properties of novel lead-free poly(vinylidene fluoride-trifluoroethylene)-Bi_{0.5}Na_{0.5}TiO₃ nanocomposite thin films for sensing applications. *Ceram Int* 41: 13836–13843
- Zeng H, Sabirianov R, Mryasov O, Yan ML, Cho K, Sellmyer DJ (2002) Curie temperature of FePt : B₂O₃ nanocomposite films. *Phys Rev B* 127:1–6
- Lee WG, Park BE, Park KE (2013) Ferroelectric properties of the organic films of poly(vinylidene fluoride-trifluoroethylene) blended with inorganic Pb(Zr, Ti)O₃. *Thin Solid Films* 546:171–175
- Xia W, Xu Z, Wen F, Zhang Z (2012) Electrical energy density and dielectric properties of poly(vinylidene fluoride-chlorotrifluoroethylene)/BaSrTiO₃ nanocomposites. *Ceram Int* 38: 1071–1075
- Chan HLW, Chan WK, Zhang Y, Choy CL (1998) Pyroelectric and piezoelectric properties of lead titanate/poly(vinylidene fluoride-trifluoroethylene) 0-3 composites. *IEEE Trans Dielectr Electr Insul* 5:505–512
- Fang M, Wang Z, Li H, Wen Y (2015) Fabrication and dielectric properties of Ba(Fe_{0.5}Nb_{0.5})O₃/poly(vinylidene fluoride) composites. *Ceram Int* 117:1–6
- Xing C, You J, Li Y, Li J (2015) Nanostructured poly(vinylidene fluoride)/ionic liquid composites: formation of organic conductive nanodomains in polymer matrix. *J Phys Chem C* 119:21155–21164
- Dias JC, Lopes AC, Magalhães B, Botelho G, Silva MM, Esperança JMSS, Lanceros-Mendez S (2015) High performance electromechanical actuators based on ionic liquid/poly(vinylidene fluoride). *Polym Test* 48:199–205
- Mejri R, Dias JC, Lopes AC, Hentati SB, Silva MM, Botelho G, Mão de Ferro A, Esperança JMSS, Maceiras A, Laza JM, Vilas JL, León LM, Lanceros-Mendez S (2015) Effect of anion type in the performance of ionic liquid/poly(vinylidene fluoride) electromechanical actuators. *Eur Polym J* 71:304–313
- Wang F, Lack A, Xie Z, Frübing P, Taubert A, Gerhard R (2012) Ionic-liquid-induced ferroelectric polarization in poly(vinylidene fluoride) thin films. *Appl Phys Lett* 100:1–6
- Liang CL, Mai ZH, Xie Q, Bao RY, Yang W, Xie BH, Yang MB (2014) Induced formation of dominating polar phases of poly(vinylidene fluoride): positive ion–CF₂ dipole or negative ion–CH₂ dipole interaction. *J Phys Chem B* 118:9104–9111
- Grimme S (2011) Density functional theory with London dispersion correction. *WIREs Comput Mol Sci* 1:211–228
- Clark T, Koch R (1999) The chemist's electronic book of orbitals. Springer, Heidelberg
- Sarkar R, Kundu TK (2018) Density functional theory studies on PVDF/ionic liquid composite systems. *J Chem Sci* 130:115
- Levine IN (2012) Quantum chemistry, 7th edn. Pearson, New York
- Bader RFW (1998) A bond path: a universal indicator of bonded interactions. *J Phys Chem A* 102:7314–7323
- García-Revilla M, Francisco E, Popelier PLA, Pendas AM (2013) Domain-averaged exchange-correlation energies as a physical underpinning for chemical graphs. *ChemPhysChem* 14:1211–1218
- Spackman MA, Byrom PG (1997) A novel definition of a molecule in a crystal. *Chem Phys Lett* 267:215–220
- C-García J, Johnson ER, Keinan S, Chaudret R, Piquemal JP, Beratan DN, Yang W (2011) NCIPLOT: a program for plotting noncovalent interaction regions. *J Chem Theory Comput* 7:625–632
- Ma W, Zhang J, Wang X (2008) Formation of poly(vinylidene fluoride) crystalline phases from tetrahydrofuran/N,N-dimethyl formamide mixed solvent. *J Mater Sci* 43:398–401
- Tomasi J, Persico M (1994) Molecular interactions in solution: an overview of methods based on continuous distributions of the solvent. *Chem Rev* 94:2027–2094
- Scalmani G, Frisch MJ (2010) Continuous surface charge polarizable continuum model solvation. 1. General formalism. *J Chem Phys* 132:114110 1–15
- Frisch M, Trucks G, Schlegel H, Scuseria G, Robb M, Cheeseman J, Scalmani G, Barone V, Mennucci B, Petersson GJ, Fox DJ (2009) Gaussian 09, revision a.01. Gaussian Inc, Wallingford
- Dennington R D, Ketith T A, Millam J M (2008) GaussView 5.0.8. Gaussian Inc, Wallingford
- Becke AD (1993) A new mixing of Hartree–Fock and local density-functional theories. *J Chem Phys* 98:1372
- Lee C, Yang W, Parr RG (1988) Development of the Colle–Salvetti correlation-energy formula into a functional of the electron density. *Phys Rev B* 37:785–789
- Pal S, Kundu TK (2013) DFT-based inhibitor and promoter selection criteria for pentagonal dodecahedron methane hydrate cage. *J Chem Sci* 125:1259–1266

36. Řezáč J, Hobza P (2016) Benchmark calculations of interaction energies in noncovalent complexes and their applications. *Chem Rev* 116:5038–5071
37. Duijneveldt FBV, Duijneveldt-van JGCMV, Lenthe JHV (1994) State of the art in counterpoise theory. *Chem Rev* 94:1873–1885
38. Jeziorski B, Moszynski R, Szalewicz K (1994) Perturbation theory approach to intermolecular potential energy surfaces of van der Waals complexes. *Chem Rev* 94:1837–1930
39. Parrish RM, Burns LA, Smith DGA, Simmonett AC, DePrince AE, Hohenstein EG, Bozkaya U, Sokolov AY, Di Remigio R, Richard RM, Gonthier JF, James AM, McAlexander HR, Kumar A, Saitow M, Wang X, Pritchard BP, Verma P, Schaefer HF, Patkowski K, King RA, Valeev EF, Evangelista FA, Turney JM, Crawford TD, Sherrill CD (2017) Psi4 1.1: an open-source electronic structure program emphasizing automation, advanced libraries, and interoperability. *J Chem Theory Comput* 13(7):3185–3197
40. Ho J, Erton MZ (2016) Calculating free energy changes in continuum solvation models. *J Phys Chem B* 120:1319–1329
41. Solymar L, Walsh D, Syms RRA (2014) *Electronic properties of materials*, 9th edn. Oxford University Press, Oxford
42. Zhan CG, Nichols JA, Dixon DA (2003) Ionization potential, electron affinity, electronegativity, hardness, and electron excitation energy: molecular properties from density functional theory orbital energies. *J Phys Chem A* 107(20):4184–4195
43. Tsuneda T, Song JW, Suzuki S, Hirao K (2010) On Koopmans' theorem in density functional theory. *J Chem Phys* 133:174101–174109
44. Parr RG, Yang W (1989) *Density-functional theory of atoms and molecules*. Oxford University Press, New York
45. Pal S, Kundu TK (2013) Stability analysis and frontier orbital study of different glycol and water complex. *ISRN Phys Chem* 2013: 753139
46. Lu T, Chen F (2012) Multiwfn: a multifunctional wavefunction analyzer. *J Comput Chem* 33:580–592
47. Guillaumes L, Salvador P, Simon S (2014) A fuzzy-atom analysis of electron delocalization on hydrogen bonds. *J Phys Chem A* 118: 1142–1149
48. Spackman MA, Jayatilaka D (2009) Hirshfeld surface analysis. *CrystEngComm* 11:19–32
49. Humphrey W, Dalke A, Schulten K (1996) VMD: visual molecular dynamics. *J Mol Graph* 14:33–38
50. Elyukhin VA (2016) *Statistical thermodynamics of semiconductor alloys*. Elsevier, Waltham
51. Irikura KK (2002) Thermo. Pl. National Institute of Standards and Technology, Gaithersburg, MD
52. Hasegawa R, Takahashi Y, Chatani Y, Tadokoro H (1971) Crystal structures of three crystalline forms of poly(vinylidene fluoride). *Polym J* 3:600–610
53. Wang ZY, Fan HQ, Su KH, Wen ZY (2006) Structure and piezoelectric properties of poly(vinylidene fluoride) studied by density functional theory. *Polym J* 47:7988–7996
54. Wu C, Visscher AD, Gates ID (2018) Interactions of biodegradable ionic liquids with a model naphthenic acid. *Nat Sci Rep* 8:176
55. Bondi A (1964) van der Waals volumes and radii. *J Phys Chem* 68: 441–451
56. Bahadur I, Kgomotso M, Ebenso EE, Redhi G (2016) Influence of temperature on molecular interactions of imidazolium-based ionic liquids with acetophenone: thermodynamic properties and quantum chemical studies. *RSC Adv* 6:104708–104723
57. Andersson MP, Uvdal P (2005) New scale factors for harmonic vibrational frequencies using the B3LYP density functional method with the triple- ζ basis set 6-311+G(d,p). *J Phys Chem A* 109:2937–2941
58. Ramer NJ, Marrone T, Stiso KA (2006) Structure and vibrational frequency determination for α -poly(vinylidene fluoride) using density-functional theory. *Polym J* 47:7160–7165
59. Katsyuba SA, Zvereva EE, Vidis A, Dyson PJ (2007) Application of density functional theory and vibrational spectroscopy toward the rational design of ionic liquids. *J Phys Chem A* 111:352–370
60. Shalu CSK, Singh RK, Chandra S (2003) Thermal stability, complexing behavior, and ionic transport of polymeric gel membranes based on polymer PVdF-HFP and ionic liquid, [BMIM][BF₄]. *J Phys Chem B* 117:897–906
61. Nalwa HS (1995) *Ferroelectric polymers: chemistry, physics and applications*. Dekker, New York
62. Jeon Y, Sung J, Seo C, Lim H, Cheong H, Kang M, Moon B, Ouchi Y, Kim D (2008) Structures of ionic liquids with different anions studied by infrared vibration spectroscopy. *J Phys Chem B* 112: 4735–4740
63. Cammi R, Cappelli C, Corni S, Tomasi J (2000) On the calculation of infrared intensities in solution within the polarizable continuum. *J Phys Chem A* 104:9874–9879
64. Yuan C, Yu H, Jia M, Su P, Luo Z, Yao J (2016) A theoretical study of weak interactions in phenylenediamine homodimer clusters. *Phys Chem Chem Phys* 18:29249–29257
65. Kerelson M, Zerner MC (1990) On the $n-\pi^*$ blue shift accompanying solvation. *J Am Chem Soc* 112:9405–9406
66. Kumar PSV, Raghavendra V, Subramanian V (2016) Bader's theory of atoms in molecules (AIM) and its applications to chemical bonding. *J Chem Sci* 10:1527–1536
67. Olmo L, Morera-Boado C, Lopez R, Garcia de La Vega JM (2014) Electron density analysis of 1-butyl-3-methylimidazolium chloride ionic liquid. *J Mol Model* 20:2175 1–10
68. Venkataraman NS, Suvitha A, Kawazoe Y (2017) Intermolecular interaction in nucleobases and dimethyl sulfoxide/water molecules: a DFT, NBO, AIM and NCI analysis. *J Mol Graph Model* 78:48–60
69. Yoosefian M, Etminan N (2016) The role of solvent polarity in electronic properties, stability and reactive trend of a tryptophane/Pd doped SWCNT novel nanobiosensor from polar protic to non-polar solvents. *RSC Adv* 6:64818–64825
70. Jablonski M (2018) Bond paths between distant atoms do not necessarily indicate dominant interactions. *J Comput Chem* 39:2183–2195
71. Foroutan-Nejad C, Shahbazian S, Marek R (2018) Toward a consistent interpretation of the QTAIM: tortuous link between chemical bonds, interactions, and bond/line paths. *Chemistry* 20:10140–10152
72. Garcia-Revilla M, Popelier PLA, Fransisco E, Pendas AM (2011) Nature of chemical interactions from the profiles of electron delocalization indices. *J Chem Theory Comput* 7:1704–1711
73. Mayer I, Salvador P (2009) Effective atomic orbitals for fuzzy atoms. *J Chem Phys* 130:234106
74. Jablonski M, Sadlej AJ (2007) Blue-shifting intermolecular C–H \cdots O interactions. *J Phys Chem A* 111:3423–3431
75. Hobza P, Havlas Z (2002) Improper, blue-shifting hydrogen bond. *Theor Chem Accounts* 108:325–334
76. Hobza P, Havlas Z (2000) Blue-shifting hydrogen bonds. *Chem Rev* 100:4253–4263
77. Hobza P, Spirko V (1998) Anti-hydrogen bond in the benzene dimer and other carbon proton donor complexes. *J Phys Chem A* 102(15):2501–2504

Publisher's note Springer Nature remains neutral with regard to jurisdictional claims in published maps and institutional affiliations.